SYNTHESIS AND NEAR INFRARED LUMINSCENT PROPERTIES OF LANTHANIDE COMPLEXES

by

Jian Zhang

B.S., Lanzhou University, 1999

M.S., Lanzhou University, 2002

Submitted to the Graduate Faculty of

Arts and Sciences in partial fulfillment

of the requirements for the degree of

Master in Sciences

University of Pittsburgh

2006

UNIVERSITY OF PITTSBURGH

ARTS AND SCIENCES

This thesis was presented

by

Jian Zhang

It was defended on

November 9, 2004

and approved by

David H. Waldeck, Professor, Department of Chemistry

Tara Y. Meyer, Professor, Department of Chemistry

Thesis Director: Stéphane Petoud, Professor, Department of Chemistry

SYNTHESIS AND NEAR INFRARED LUMINESCENT PROPERTIES OF LANTHANIDE COMPLEXES

Jian Zhang, M.S.

University of Pittsburgh, 2006

In vivo near-infrared (NIR) fluorescence microscopy and imagery is an emerging research area in biology. Organic dyes currently tested for NIR imagery have very severe limitations such as rapid photobleaching. This drastically limits the sample exposure time and/or prevents the experiment to be repeated. Lanthanide complexes have NIR luminescence properties which have strong resistance to photo-bleaching, long luminescence lifetimes and sharp emission bands. In addition, the emission band energies are independent from the experimental condition. All these properties make them the most promising agents for NIR imagery. In this thesis, it was demonstrated that tropolonate ligands can be used as an efficient sensitizer for several luminescent lanthanide cations (Nd, Ho, Er, Tm, Yb) emitting in the NIR. One octadentate ligand was developed to fulfill the complete coordination requirements of lanthanide cations in order to achieve increased stability of the complex to sustain physiological conditions to maximize the protection of the coordinated lanthanide cation against non-radiative deactivation. To study and rationalize the mechanism of ligand to lanthanide of energy transfer, derivatives of tropolone and their corresponding complexes are synthesized. The mechanism of the energy transfer can be used to design lanthanide complexes with controlled properties.

TABLE OF CONTENTS

LIST OF TABLES

LIST OF FIGURES

ACKNOWLEDGEMENTS

I consider myself extremely fortunate to have had the amazing opportunity to work for my advisor, Professor Stéphane Petoud. His enthusiasm and passion for the lanthanide chemistry make him an inspirational and exceptional teacher. I thank him for his infinite patience, guidance and motivation over these past few years.

Thank you to all the members of the Petoud group along with all my friends in the department. This includes, but is not limited to Dr. Paul Badger, Dr. Jason Cross, Demetra Chengelis, Adrienne Yingling, Grzegorz Filipczyk, Hyounsoo Uh, David Oxley, and Chad Shade.

Finally, I would like to thank my family for their life-long support.

1.0 INTRODUCTION

The noninvasive visualization of specific molecular targets, pathways and physiological effects *in vivo* is in great demand in the life science. Many advances in fluorescent probes, fluorescent proteins and imaging technologies allow for the examination the structure and function of cells.[1] Near infrared (NIR) fluorescence imaging is the most promising technology for *in vivo* imaging with high resolution.

In biomedical imaging, an excitation photon typically travels through the tissue to reach the fluorescent agent, and the photon emitted by the fluorophore travels back and is collected by the detector. Both excitation and emission photon have several fates, such as absorption by tissue or organ, scattering and auto fluorescence arising from the emission from the biological serum.[2] Near infrared light from 700 nm to 1100 nm is used because it minimized all three fates. Firstly, tissue (skin, blood etc) has low absorption in this range.[3] Typical absorption spectrum of blood and skin is showed in Figure 1.

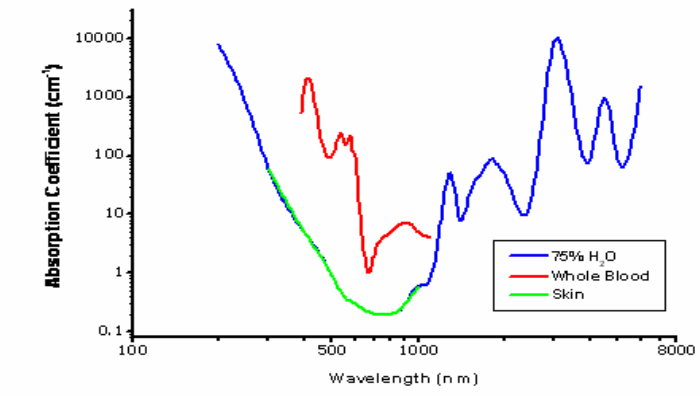

Figure 1. Absorption spectra of kin and whole blood.

Secondly, NIR light has limited scattering (proportional to $1/\lambda^4$). Light scattering describes the deviation of a photon from the parallel axis of its path, and can occur when the tissue inhomogeneity is small (Rayleigh scattering), or roughly equal (Mie scattering) to wavelength.[2] Increased scattering leads to reduced resolution of the image. Thirdly, when NIR light is used, the autofluorescence can be eliminated because biological molecules seldom have fluorescence in NIR range. As a consequence, the fluorescence background is reduced and the sensitivity of the measurement is increased. Figure 2 shows the autofluorescence spectra at different excitation wavelengths.

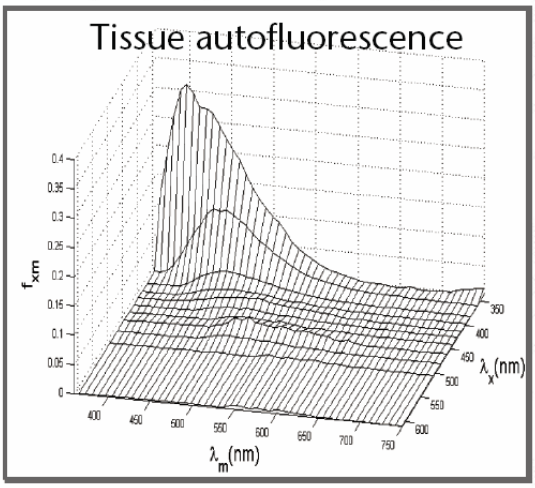

Figure 2. 3-D spectra of tissue autofluorescence.[1]

Currently, the main type of NIR fluorescence agents used in biological imaging is organic fluorophores. One important class of these is the heptamethine cyanines. Of these, the indocyanines are the most widely used. They have typically 760-800 nm absorption band and 790-830 nm emission band.[2] Figure 3 is an example of one recently developed heptamethine indocyanine. Tetra-sulfonation in this compound increases aqueous solubility and aqueous quantum yield. Up to now several fluorophores of this type and their conjugation chemistry have been reported (Figure 4).[4-6]

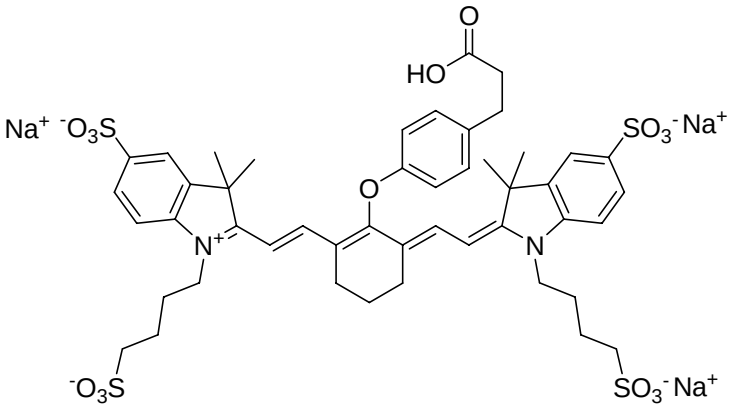

Figure 3. Carboxylic acid form of IRDye78: a tetra-sulfonated indocyanine.

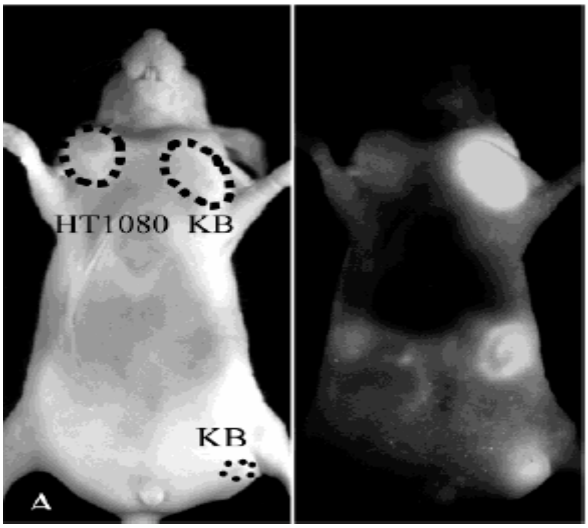

Figure 4. In vivo imaging of folate receptor. The folate has been conjugated to the indocyanine dye.[4]

Although the conventional organic fluorophores have good solubility (due to appropriate functionalization) and reasonable quantum yield (3% to 15% in aqueous solution)[2], they suffer from major limitations. The excitation and emission wavelength are strongly dependant from the experimental conditions, and more importantly, organic fluorophores in general are highly susceptible to photobleaching, which limits the number of photons per unit of time and surface (fluence rate) that can be applied to a sample, and hence the sensitivity of detection. For example, heptamethine indocyanines rapidly photobleach (in seconds) in serum when fluence rate exceeds 50

mW/cm^2.[7] This prevents long and repeated exposure of the sample to light, which is a major limitation for biological imaging and fluorescence microscopy. This also explains that despite the significant advantages of their NIR emission, very few applications are taking advantage of organic NIR fluorophores.

Recently, considerable work has been done with inorganic fluorescent semiconductor nanocrystals (quantum dots) for biological imaging, which have the potential to solve some problems of the conventional organic fluorophores.[8] Quantum dots (QD) are synthesized in organic solvents. They are typically constituted from an inorganic core (CdSe or CdTe) and inorganic outer shell of metal (ZnS). The emission wavelength can be tuned by controlling the size of the nanoparticles. To be used *in vivo*, they must be coated with an aqueous-compatible organic layer. They have good photophysical properties: broadband absorption and the absorption coefficient increases when wavelength is smaller. This allows multiple quantum dots with different fluorescence emission wavelengths to be excited using the same wavelength. High quantum yield (up to 50%-60% for quantum dots with organic coating in aqueous solution[2]), and good resistance to photobleaching make them very good candidates for *in vivo* imaging.

However, quantum dots have intrinsic limitations. First, they are large particles when compared to the organic fluorophores or even to cells. Typical size for NIR emitting QDs is about 20 nm with the coating. This limits their application in many areas of *in vivo* imaging, especially, for cellular imaging. Since their large size relative to the cell may prevent them to penetrate in all regions of the cell. Secondly, quantum dots are constituted of highly toxic elements such as Cadmium, Selenium and Tellurium, which most probably will prevent their use for application *in vivo* by

FDA. The oxidation effect on the quantum dots can liberate the toxic Cd^{2+} ions in the cell has been reported recently.[9]

Considering the drawbacks of both organic flurophores and quantum dots, new NIR fluorescent agents are in high demand. NIR luminescent lanthanide complexes have the potential to be the promising candidate to be a new member of NIR fluorescent agent in bioimaging.

Lanthanides are the elements starting from Cerium (Z = 58) to Lutetium (Z = 71), which are located in the first row of *f*-block in the periodic table. The lanthanides usually form cations with a 3+ charge. The *f* orbitals are higher in energy than 5*s* and 5*p* orbitals, but spatially shielded by the outer 5*s* and 5*p* orbitals. This special electronic configuration gives them very unique photophysical properties.[10] First, the transitions with the *f*-orbital manifold are parity forbidden, which leads to low molar absorption coefficients in the order of 10 $cm^{-1}mol^{-1}$ and long lifetime (up to several milliseconds) of the excited states and resulting luminescence. Secondly, the 4*f* orbitals are hardly affected by the surrounding environment and not involved in bonding, which make the transitions (either absorption or emission) relatively located at fixed wavelength and line-like (atom like). Lanthanide ions with completely filled (Lu^{3+}) and half-filled (Gd^{3+}) 4*f* orbitals are not luminescent. The latter is not luminescent because of its highly located excited states. The other ions have a large number of electronic levels and the luminescence ranges from the UV to the NIR. The energy level diagram for lanthanide ions is shown in Figure 5.

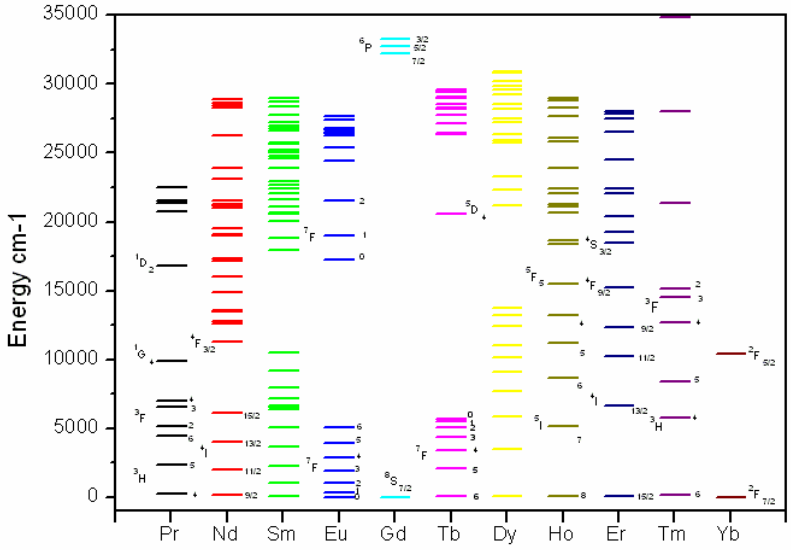

Figure 5. Energy level diagram of electronic levels associated with the 4f orbital of selected lanthanide ions.

Due to the low molar absorption coefficient of lanthanide ions, the direct excitation of their electronic states is not efficient. In 1942, Weissman discovered that sensitized emission from the lanthanide ions can be achieved via absorption of a suitable organic ligand followed by energy transfer to the metal center.[11] To date several visible emitting lanthanide complexes have been used in practical applications such as luminescent markers in bioassay diagnostic imagery[12, 13] and homogeneous time-resolved immunoassays[14, 15].

The development of NIR emitting lanthanide complexes based on Nd, Yb and Er has received much attention in recent years. The luminescence of Yb, Nd, Ho and Tm have emission bands ranging from 800 nm to 1100 nm, which is suitable for the application related to *in vivo* imaging, because the biological tissue has low absorption at this range of wavelength. Typically, these complexes display long lifetime (μs to ms) in comparison to the organic fluorophores (ps to ns), allowing for their uses in time-resolved experiments. Emission bands of lanthanide are much

narrower than the organic fluorophores and quantum dots. This is very useful in the application of multiplex imaging because the emission of several lanthanides can be quantified during the same experiment. In addition, advances in two and three-photon laser technologies allow the excitation of molecules absorbing in an energy range from 400-500 nm, and even 315 nm by using NIR excitation light, which can penetrate deeply into tissues.[16-18] Also, NIR light has reduced photo-toxicity to biological cells and tissues in comparison to UV light.

1.1 PHOTOPHYSICS OF LUMINESCENT LANTHANIDE COMPLEXES

A luminescent lanthanide complex consists of a lanthanide ion coordinated by the ligand(s). In most cases, the ligand contains a light-absorbing group in the form of an organic chromophore. Such group is generally referred to as the "antenna" chromophore.[19] The photonic energy absorbed by this antenna can be transferred to the encapsulated lanthanide ion, and sensitize its luminescence. This process is referred to "antenna effect" and is illustrated in Figure 6.

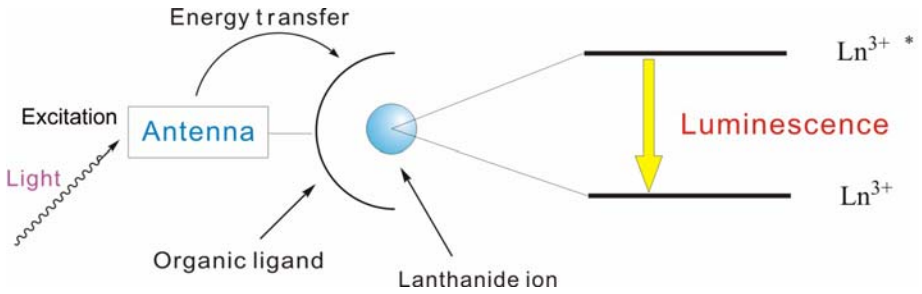

Figure 6. Photosensitization: Antenna effect.

Although there are some examples showing that the energy can transfer from the singlet states[20, 21], most of the luminescent lanthanide complexes have been reported as following the mechanism of photosensitization from triplet states of ligand. This process is showed in Figure 7. Excitation of the antenna into its singlet-

singlet transition is followed by intersystem crossing (ISC) which results in population of the antenna's triplet state. From the triplet excited antenna, the energy migrates to the lanthanide ion.[22, 23] ISC competes with other processes that occur from the antenna's singlet state, particularly fluorescence. Also there are some other processes that deactivate the antenna triplet state, such as quenching by molecular oxygen which has a triplet ground state. So the overall quantum yield of the lanthanide luminescence (Φ_{tot}) that is excited via the antenna chromophore, is dependent on the product of quantum yields of the individual three steps: intersystem crossing, (Φ_{ISC}), energy transfer (Φ_{ET}) and lanthanide luminescence (Φ_{Ln}).

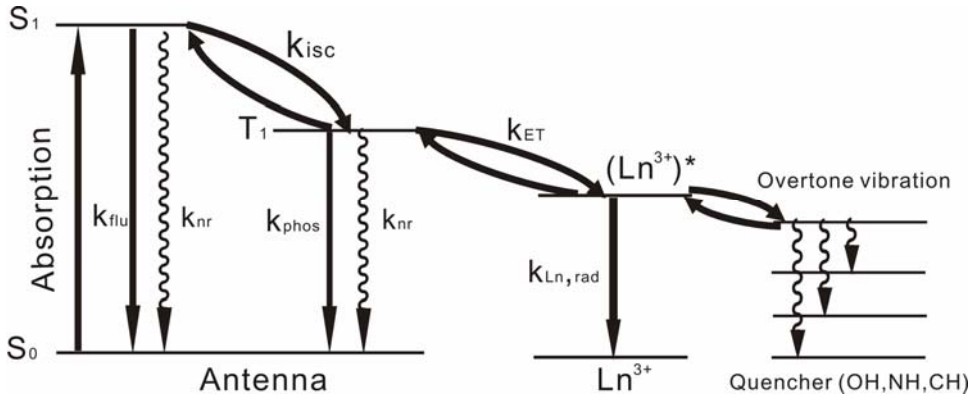

Figure 7. Jablonski diagram for sensitized Ln^{3+} emission (k_{flu}, rate of fluorescence; k_{ISC}, intersystem crossing rate; k_{phos}, phosphorescence rate; k_q, triplet quenching rate; k_{nr}, non-adiative decay rate; k_{ET}, energy transfer rate; and $k_{Ln,rad}$, radiative decay rate.).

Two main mechanisms have been proposed for the process of energy transfer from the triplet state of the ligand to the metal center. The Förster mechanism is a dipole-dipole interaction between the donor and acceptor.[24, 25] The absorption spectrum of the energy acceptor and the emission spectrum of the energy donor must overlap for this to occur. This mechanism takes place through space, the efficiency is dependent on r^{-6}, where r is the distance between the donor and acceptor. The second mechanism is called as Dexter mechanism, which is an electron-exchange mechanism.[26] It requires electron exchange between the donor and acceptor, and

therefore the direct contact and spin-orbit coupling are essential. Simultaneous exchange of electrons is required and the efficiency is proportional to e^{-r}, where r is the distance between the donor and acceptor.

Besides these two mechanisms proposed for energy transferred from triplet states, in some cases, a sequential electron exchange mechanism has been used to explain the energy transfer in complexes of Eu^{3+} and Yb^{3+}, which can be easily reduced (Figure 8).[27-29] This mechanism is favorable in cases where there is poor overlap between the electron transfer step is thermodynamically feasible, which in turn depends upon the oxidation potential of the excited state of the donor and the reduction potential of the metal ion.

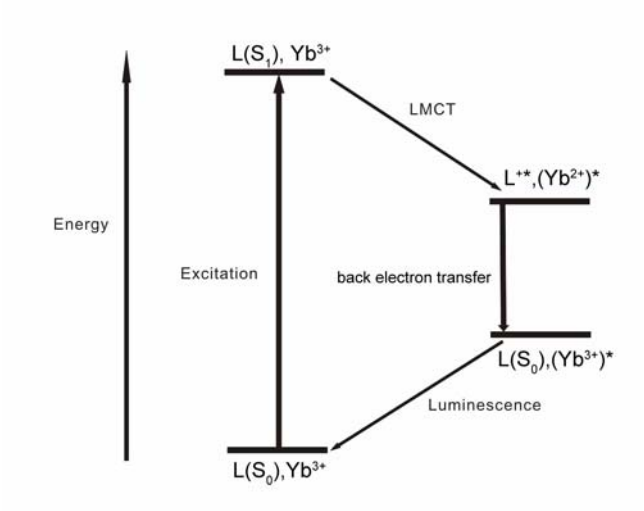

Figure 8. Representation of sequential electron transfer mechanism.

Energy gap between the lowest excited state and ground state is another important aspect in photophysical properties in lanthanide complexes.[30, 31] The excited state of lanthanide cation can be rapidly deactivated by the overtones of high frequency vibrations through non-radiative processes such as O-H, N-H, and C-H oscillations.[32] This type of quenching effect is much more pronounced for NIR lanthanide ions, because of the smaller energy gap between the excited and ground states (Figure 9). For example, two quanta of OH vibration will quench the lowest

excited state of Nd^{3+}, but three to four quanta of OH vibration are needed to quench those of Eu^{3+}.

To summarize, in order to obtain highly luminescent lanthanide complexes, the following requirements have to be fulfilled.

• The ligand(s) have to bind the lanthanide ions tightly (oxygen donor ligand are preferred because of its hard base properties) and complete the requirement of high coordination number of lanthanide ions in solution (usually 8 to 10).

• The ligand must have appropriate energies of singlet and triplet states, and have a good energy match with the excited state energy level of lanthanide ions to achieve good energy transfer.

• The ligand should be modified easily so the properties, such as photophysical, thermodynamical and solubility, can be controlled.

• Functionalities that allow conjugation to proteins, such as proteins, antibodies, and DNA are needed for use in specific biological applications.

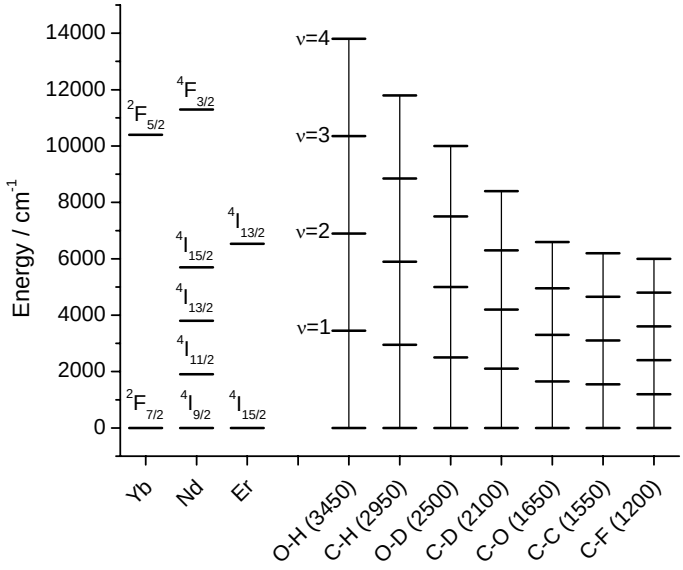

Figure 9. Radiative transition energies of Yb^{3+}, Nd^{3+}, and Er^{3+} and the vibrational energies of common bonds found in organic systems.

Up to now, there have been only few reports of NIR lanthanide complexes. Selected NIR luminescent lanthanide complexes are shown in Figure 10 and Table 1. Verhoeven *et al.* used an amino-carboxylate derivative (1) based on fluorescein as a sensitizer and prepared the corresponding Yb complex. This complex was tested in an NIR fluoroimmunoassay, and to date this is the only example of NIR emitting lanthanide complex used in a practical assay.[33] Van Veggel *et al.* synthesized a series of ligands (2, 3) based on *m*-terphenyl group. They attached organic dyes and red-emitting Ru complexes to that group and used them as the sensitizer of the NIR emitting cations.[34, 35] Faulkner *et al.* used DO3A type ligands (4, 5, 6), covalently or non-covalently bonded to a chromophore, and studied the luminescence properties of these complexes.[36-38] Yanagida *et al.* studied the luminescent properties of the Nd^{3+} complexes using deuterated and fluorinated *β*-diketone (7, 8) as ligands, and these two ligands were designed to minimize the high energy vibrations of C-H.[39] Besides, Bünzli, Ward, Wong and Schanze also have investigated NIR emitting lanthanide complexes.[40-44] Most of the complexes have relatively low quantum yields, this might due to the poor protection and inefficient energy transfer. To date, only Nd and Yb have been studied as NIR luminescent lanthanide reporters. A lot of work needs to be done to prepare better lanthanide complexes which can be applied in the NIR fluorescence imaging. Other luminescent lanthanide ion with different emission bands such as Ho^{3+} and Tm^{3+} have potential as NIR reporter, which is beneficial for multiplex assays.

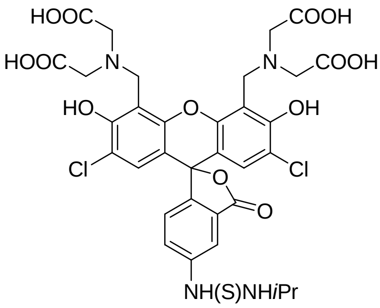

1

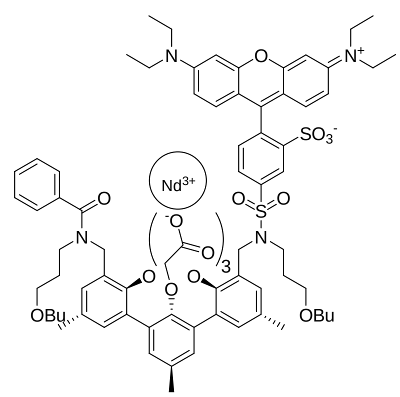

2

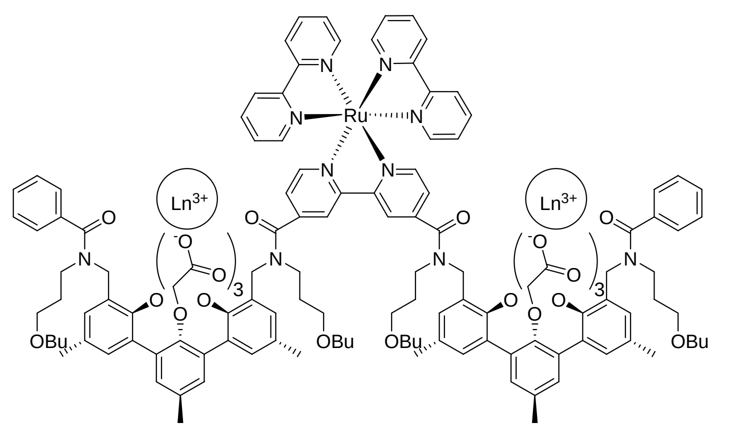

3

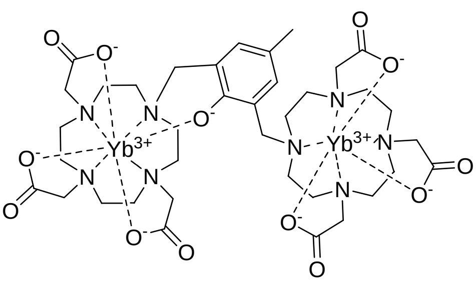

4

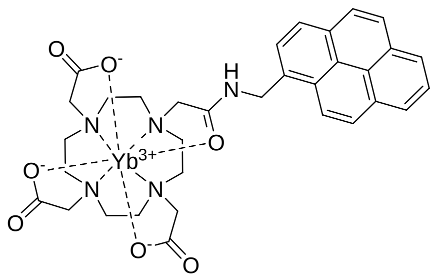

5

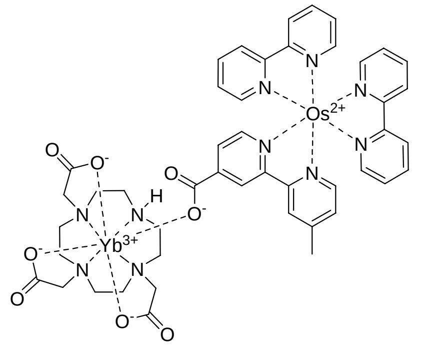

6

7 8

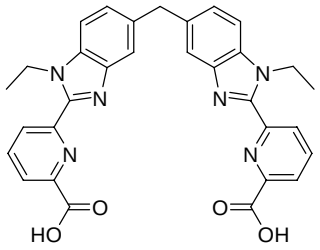

9

Figure 10. Selected ligands that form luiminescent complexes in the NIR and complexes emitting in the NIR Continuation.

Table 1. Selected of NIR luminescent lanthanide complexes in literature.

ligand	ion	solvent	λ_{max}/nm	$\varepsilon_{max}/M^{-1}cm^{-1}$	Φ_{tot}	$\tau_{obs}/\mu s$	ref
1	Yb	aqueous buffer	516	145,000	5.34E-4	1.8	[33]
2	Nd	d_6-DMSO	455			2.1	[35]
	Yb					18.2	[35]
3	Nd	d_6-DMSO	570	88,000		2.21	[34]
4	Yb	H_2O				1.67, 0.51	[36]
		D_2O				4.95, 1.17	[36]
5	Yb	H_2O				1.34	[37]
		D_2O				7.40	[37]
6	Yb	CH_3OH				1.38	[38]
		CH_3OD				8.192	[38]
7	Nd	d_6-DMSO			0.033[a]	13[b]	[39]
8					0.032[a]		[39]
9	Yb	D_2O	310		0.018	40	[40]

a. Direct excitation of Nd ion.
b. Quantum yield in d_6-Acetone

1.2 OUR WORK

The core of this work concerns the photosensitization of NIR luminescent lanthanide cations. Chapter 2 discusses a new type of ligand, tropolone, and lanthanide complexes formed with this ligand. The structure and luminescent properties of the complexes were investigated. Chapter 3 is one of the extension of the work presented in chapter 2. We synthesized an octadentate ligand, where four tropolone chelating units are connected by common backbone to increase the thermodynamic stability. The photophysical properties of the resulting complexes were investigated. Chapter 4 presents some preliminary work that has been done on the tuning of the photophysical properties of lanthanide complexes by using functionalized tropolones. Chapter 5 presents a conclusion and some discussion of future work to be done.

2.0 SYNTHESIS AND PROPERTIES OF LANTHANIDE COMPLEXES WITH TROPOLONE

2.1 INTRODUCTION

To develop a well-protected lanthanide complex, the ligand must satisfy the requirement of high coordination number for lanthanide ions. Eight to ten is the common coordination number for a well-protected lanthanide ion in solution. Either a multidentate ligand (e.g. DPTA) or several bidentate/tridentate ligands could be used.[45] In addition, given the hard lewis acid character of lanthanide cations, it is more favorable to use hard lewis base ligands, best being oxygen donor ligands, such as carboxylic acids, β-diketone etc, to form strong bonds between the metal ions and the ligand(s). Last, from an energy transfer point of view, the energy of the triplet state of the ligand should match the excited energy level of lanthanide cation.

Ligands incorporating organic fluorescent dyes[33], luminescent ruthenium bipyridine complexes[34, 46], and porphyrins[41, 42] have been used as the sensitizer for NIR luminescent lanthanide complexes. They have one common property, low energy level of triplet states, which is beneficial for NIR emitting lanthanide ions because their excited states are also low in energy. For example, the lowest excited energy level for Nd^{3+} is 11,527 cm^{-1}, for Er^{3+} is 6,610 cm^{-1}, and for Yb^{3+} is 10,100 cm^{-1}.

Tropolone (2-hydroxycyclohepta-2,4,6-trienone) is a seven-membered ring ligand as shown in Figure 12. It has a pKa value 6.7,[47] allowing for deprotonation at physiological pH, and is a good chelator for metal ions. In most tropolone metal

complexes, the deprotonated hydroxyl group and carbonyl oxygen are involved in the coordination to the metal ion, resulting in a bidentate complex. This forms an energetically-favorable five-membered chelate ring. The coordination chemistry of tropolone with various metal ions has been studied. Muetterties *et al.*[48] have studied the coordination chemistry of tropolone with lanthanide ions. By using different synthetic conditions, they isolated two types of complexes with different stoichiometry: ML_3 and ML_4. The formulas of theses complexes were supported by elemental analysis, but X-ray crystal structures have not been reported. The electronic structure of tropolone have also been studied.[49, 50] It has been found that tropolone has a low-lying triplet state at 16,800 cm^{-1} (595 nm).[51] In view of these two unique properties of tropolone: strong binding to lanthanide and low energy-lying triplet state, we synthesized the LnL_4 complexes and studied their luminescent properties. For the first time, X-ray quality single crystals for LnL_4 complexes were obtained with Ln = Tb, Dy, Ho, Er, Tm, Yb and Lu. The NIR luminescence from Yb^{3+}, Nd^{3+}, Er^{3+}, Tm^{3+} and Ho^{3+} complexes were observed, and as far as we know, this is the first report of the luminescence of a Ho^{3+} complex in solution.

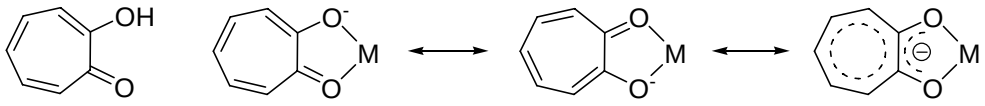

Figure 11. Structure of tropolone ligand and its coordination mode with metal ion.

2.2 EXPERIMENTAL SECTION

2.2.1 Chemicals

All reagents were used as received, unless otherwise stated. Tropolone, $LnCl_3 \cdot nH_2O$ (Ln = La, Nd, Eu, Gd, Er and Yb, 99.9% or 99.99%, n = 6 or 7), $YCl_3 \cdot 6H_2O$ (99.99

%) and KOH solution in methanol (0.103 N) were purchased from Aldrich. $LnCl_3 \cdot nH_2O$ (Ln = Pr, Sm, Tb, Dy, Ho, Tm and Lu, 99.9% or 99,99%, n = 6 or 7) were bought from Strem Chemicals. Quinine sulfate (99.0%) was purchased from Fluka. All deuterated NMR solvents were purchased from Cambridge Isotope Labs and used as received.

2.2.2 Physical measurements

Melting points were measured on a Fisher-Johns melting pointer apparatus and were uncorrected. Infrared spectra were recorded on a Perkin-Elmer Spectrum BX FT-IR. Polystyrene film was used as the external standard (1601 cm^{-1} peak). Elemental analyses were performed by Atlantic Microlab, Inc. ^1H NMR spectra were recorded on a Bruker DPX-300 at 300 MHz. MS-EI and MS-ESI were measured on a Micromass Autospec and Agilent HP 1100 series LC-MSD respectively. Absorption spectra were recorded on a Perkin-elmer Lamda 9 spectrophotometer. Metal cation luminescence emission and excitation spectra were measured using a modified Jobin Yvon-Spex Fluorolog-322 spectrofluorometer equipped for both room temperature (RT) and 77 K measurements. Luminescence and excitation spectra were corrected for the instrumental function. Ligand fluorescence quantum yields were measured using quinine sulfate in 0.1 N H_2SO_4 (Φ = 0.546) as reference.[52] Metal cation luminescence quantum yield were measured using the $^4G_{5/2} \rightarrow {}^6H_{9/2}$ transition of a Sm(2-hydroxy- isophthalamide macrobicycle) previously reported ($\Phi = 7.3 \cdot 10^{-4}$ in 0.01 M TRIS buffer) as reference.[53] The use of a Sm^{3+} complex allows for a simple method of cross calibrating the visible detector with the NIR detector of the Fluorolog-322. The quantum yields were calculated using the following equation:

$$\Phi_x/\Phi_r = [A_r(\lambda_r)/A_x(\lambda_x)][I(\lambda_r)/I(\lambda_x)][\eta_x^2/\eta_r^2][D_x/D_r]$$

in which subscript *r* stands for the reference and *x* for the sample; *A* is the absorbance at the excitation wavelength, *I* is the intensity of the excitation light at the same wavelength, η is the refractive index (η = 1.333 in H_2O, η = 1.479 in DMSO), and *D* is the measured integrated luminescence intensity.

The lifetime measurements were performed by excitation of solutions in 1 cm quartz cells using a nitrogen laser (Oriel model 79110, wavelength 337.1 nm, pulse width at half-height 15 ns, 5-30 Hz repetition rate). Emission from the sample was collected at a right angle to the excitation beam by a 3" plano-convex lens. Emission wavelengths were selected by means of quartz filters. The signal was monitored by a cooled photomultiplier (Hamamatsu R316) coupled to a 500 MHz bandpass digital oscilloscope (Tektronics TDS 754D). The signals (15,000 points each trace) from at least 500 flashes were collected and averaged. Background signals were similarly collected and subtracted from sample signals. Lifetimes are averages of at least three independent determinations. Data were fitted to exponential decay by OriginPro (V7 SP4) data analysis and linefitting software. Ligand-centered triplet state lifetimes were performed by excitation of solid samples in a quartz tube at 77 K using the nitrogen laser described previously. Emission from the samples was collected at a right angle to the excitation beam, and the emission wavelengths were selected by means of a Spex FL1005 double monochromator. The signal was monitored by a Hamamatsu R928 photomultiplier coupled to a 500 MHz bandpass digital oscilloscope (Tektronics TDS 620B). The signals (15000 points each trace) from at least 500 flashes were collected and averaged. Background signals were similarly collected and subtracted from sample signals. Lifetimes results from at least three time independent determinations.

X-ray crystallography

Crystals suitable for X-ray crystallographic study were coated with Fluorolube® then mounted on a glass fiber and coated with epoxy cement. X-ray data were collected on a Bruker Apex diffractometer using graphite monochromatized Mo Kα radiation (λ = 0.71073 Å). Data collection was controlled using the Bruker SMART program, and the data processing were done with the SHELXTL program package[54-56], and the graphics was done by using Ortep-3,[57] Mercury 1.2.1[58] and Ortex[59]. All hydrogen atoms were calculated and placed in idealized positions (d_{C-H} = 0.96 Å). The diffraction studies were carried out by Dr. Steven Geib, Department of Chemistry, University of Pittsburgh.

2.2.3 Synthesis of complexes and preparation of single crystals

To a solution of tropolone (48.8 mg, 0.04 mmol) in MeOH (10 mL) was added KOH (0.04 mmol) methanol (0.100 M) with stirring. To the resulting solution was added $LnCl_3 \cdot nH_2O$ (0.01 mmol) (Ln = La, Pr, Nd, Sm, Eu, Gd, Tb, Dy, Ho, Er, Tm, Yb and Lu) or $YCl_3 \cdot 6H_2O$ in methanol (10 mL). The solution was stirred for 3 hours and the resulting precipitate was filtered, washed three times with methanol and dried *in vacuo* over P_2O_5 for 48 hours. Single crystals of $[K(LnL_4)DMF]_\infty$ were obtained from slow diffusion of diethyl ether into concentrated DMF solutions of $K(LnL_4)$.

2.3 STRUCTURE CHARACTERIZATION

2.3.1 Solid state study

2.3.2.1 Elemental analysis and IR spectra

Results of elemental analysis (Table 2) indicate that the ML_4 (metal to ligand) complexes have been isolated. All the complexes have K^+ cation, the counter ion for the $[Ln(trop)_4]^-$ anion.

The IR spectra of "free ligand" potassium tropolonate, and all the lanthanide complexes were measured (Table 2). For comparison, the IR spectrum of tropolone was also measured.

The intra-molecular H-bonded OH stretching vibration of tropolone is assigned to the broad band from 3,200 cm^{-1} to 2,500 cm^{-1}, which disappears in the potassium tropolonate and lanthanide complexes, indicating a complete deprotonation of the OH group.

Band around 1,620 cm^{-1} in tropolone was assigned to the stretching of C=O bond. After deprotonation, the C=O stretching bands red-shift 13 cm^{-1} when compared to potassium tropolonate. This shift is due to the resonance of the deprotonated tropolonate anion (Figure 12), gives the C=O bond has a single-double bond character, therefore decreasing the stretching energy. After coordination, this vibration red-shifts 10 cm^{-1} more, this is due to a further decrease of the double bond character of the C=O bond, which indicates that the oxygen atom of carbonyl groups participate in the complexation of Ln^{3+}. The stretching vibrations of C-O disappear in potassium tropolonate and complexes because the two CO vibrations are identical due to the resonance. The crystallography data also substantiates the equivalency of these two bonds. The bond length of C=O in tropolone is 1.261 Å. In the complexes, the

average C-O bond length is 1.276 Å. The same effect was observed for C=C stretching vibration, which is located at 1542 cm^{-1}, 1530 cm^{-1} and 1508 cm^{-1} in tropolone, potassium tropolonate, and lanthanide complexes respectively.

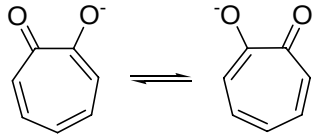

Figure 12. Resonance structure of tropolonate anion**.**

The bands around 1230 cm^{-1} and 720 cm^{-1} are the vibration of C-H bond in-plane and out-of-plane respectively. The changes in these two bands might indicate the changes of rigidity of the tropolone ring after the coordination. The metal-oxygen bond was identified in the IR spectra around 480-490 cm^{-1}. The frequency of this bond is an indication of the covalency of M-O bond and is higher in heavier lanthanide ions. This result is consistent with the previous study.[60]

Table 2. Elemental analytical and IR spectra data for complexes.

Compound	Elemental analysis (%)[a]		IR (ν_{max}/cm^{-1})[b]				
	C	H	$\nu_{C=O}$	$\nu_{C=C}$	δ_{C-H} (in plane)	δ_{C-H} (out of plane)	ν_{Ln-O}
$C_7H_6O_2$	—	—	1614	1548	1241	711	—
$C_7H_5O_2K$	—	—	1601	1530	1233	734, 716	—
$C_{28}H_{20}O_8KLa$	50.37(50.77)	3.00(3.04)	1593	1508	1221	729	481
$C_{28}H_{20}O_8KPr$	50.59(50.61)	2.98(3.03)	1592	1507	1223	731	485
$C_{28}H_{20}O_8KNd$	50.12(50.36)	3.06(3.02)	1592	1507	1225	732	487
$C_{28}H_{20}O_8KSm$	49.59(49.90)	2.94(2.99)	1591	1507	1225	733	490
$C_{28}H_{20}O_8EuK$	49.62(49.78)	2.95(2.98)	1592	1508	1226	733	492
$C_{28}H_{20}O_8GdK$	49.50(49.40)	2.89(2.96)	1592	1508	1227	734	494
$C_{28}H_{20}O_8KTb$	49.30(49.28)	2.95(2.95)	1592	1508	1227	734	495
$C_{28}H_{20}O_8DyK$	48.78(49.02)	2.92(2.94)	1592	1510	1228	735	498
$C_{28}H_{20}O_8HoK$	48.23(48.85)	2.93(2.93)	1592	1510	1229	736	499
$C_{28}H_{20}O_8ErK$	48.52(48.68)	2.86(2.92)	1592	1511	1228	737	500
$C_{28}H_{20}O_8KTm$	47.75(48.56)	2.98(2.91)	1592	1512	1229	737	502
$C_{28}H_{20}O_8KYb$	48.47(48.28)	2.92(2.89)	1592	1512	1229	737	504
$C_{28}H_{20}O_8KLu$	47.87(48.15)	2.85(2.89)	1592	1512	1230	737	505
$C_{28}H_{20}O_8KY$	54.95(54.91)	3.23(3.29)	—	—	—	—	—

[a] Data in parenthesis are theoretical values. [b] The assignment was based on the previous IR results.[61, 62]

2.3.2.2 Crystal structure

The crystallographic data for the complexes are listed in Table 3. Except Tb complex, all the other six crystal structures are isomorphous (The structure of Yb complex is shown in Figure 13 as am example). The coordination mode in all the complexes is similar. The lanthanide cation is coordinated to four tropolone ligands, and the coordination number of the lanthanide cation is eight. The average Ln-O bond length in each of these complexes ranges from 2.31 to 2.37 Å (See Table 4), and bond length decreases from Tb to Lu, which can be explained by the change in the respective ionic radii of the central ion. The K^+ bridges two $[LnL_4]^-$ units by coordinating six oxygen atoms, three from each unit, with an average K-O bonds length of 2.8 Å. In addition, there is a DMF solvent molecule coordinated to the K^+ by its carbonyl oxygen atom. The total coordination number for K^+ is seven (Figure 14, 15). Through the bridging K ions, coordination polymeric chains are formed, which have $[K(LnL_4)DMF]$ as the repeated unit. Figure 16 shows the polymeric chain of the complexes. The distance between adjacent Ln^{3+} ions and K^+ ions is approximately 3.85 Å (Table 4). The main difference between the structure of the Tb complex and the other ions is the relative position of Ln^{3+} and K^+ ions. The simplified views of the polymer chains for the two types of the complexes are shown in Figure 17. Although both of them have the zigzag motif of Ln•••K•••Ln•••K•••Ln, the two types of arrangements can be distinguished by the relative position of K^+ with the Ln•••Ln•••Ln chain. In the structures of Dy-Lu complexes, the K ions are isodentate (on the same side of Ln•••Ln•••Ln chain), but in the Tb complex, the K ions are syndiodentate (located alternatively on both side of the Tb•••Tb•••Tb chain) (Figure 17).

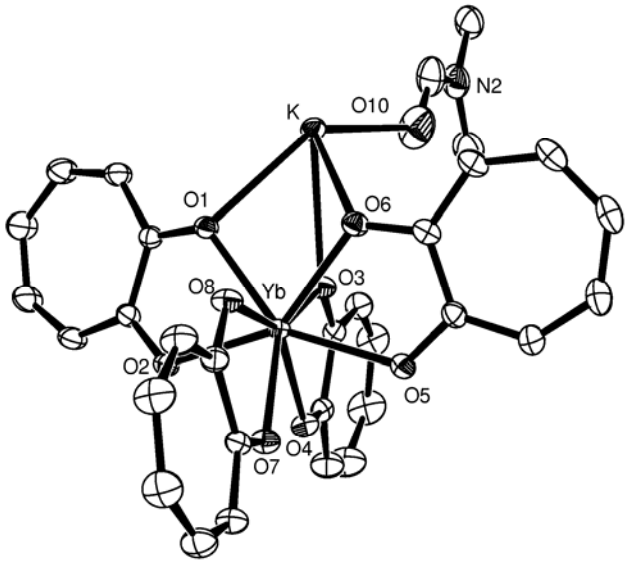

Figure 13. Molecular structure of $\{K[Yb(Trop)_4]DMF\}_{\infty}$.

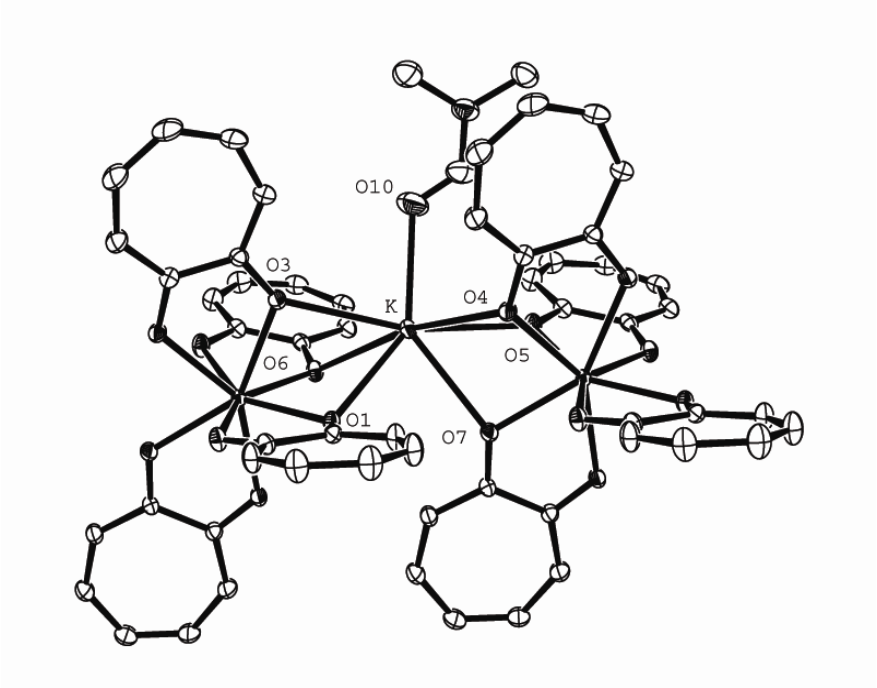

Figure 14. The coordination environment of K^+ in $\{K[Yb(Trop)_4]DMF\}_{\infty}$.

Table 3. Summary of Crystal Data for $\{K[Ln(Trop)_4]DMF\}_\infty$ (Ln = Tb, Dy, Ho, Er, Tm, Yb, Lu).

Complex	$C_{31}H_{27}O_9KTb$	$C_{31}H_{27}O_9DyK$	$C_{31}H_{27}O_9KHo$	$C_{31}H_{27}O_9ErK$	$C_{31}H_{27}O_9KTm$	$C_{31}H_{27}O_9KYb$	$C_{31}H_{27}O_9KLu$
M	755.56	759.14	761.57	763.90	765.57	769.68	771.61
Space group	$P2_1/n$	*P*-1	*P*-1	*P*-1	*P*-1	*P*-1	*P*-1
a(Å)	12.7566(12)	7.3048(5)	7.2622(4)	7.2758(10)	7.296(3)	7.2409(3)	7.2465(4)
b(Å)	13.2771(12)	11.0879(8)	10.9440(6)	10.9867(16)	11.077(4)	10.9079(4)	10.9035(5)
c(Å)	18.9393(18)	20.1174(15)	19.9951(12)	20.037(3)	20.107(7)	19.8683(7)	19.8822(10)
α(°)	90.00	79.3790(10)	80.0340(10)	79.993(3)	79.576(6)	80.0870(10)	80.1350(10)
β(°)	95.984(2)	84.2300(10)	84.0010(10)	84.103(3)	84.340(7)	84.1570(10)	84.1030(10)
γ(°)	90.00	78.8070(10)	78.8730(10)	78.941(3)	78.757(6)	78.8690(10)	78.8180(10)
V(Å^3)	3190.3(5)	1567.48(19)	1531.60(15)	1544.1(4)	1564.2(10)	1512.93(10)	1514.40(13)
Z	4	2	2	2	2	2	2
μ/mm^{-1}	2.399	2.569	2.773	2.906	3.022	3.283	3.452
T/K	295(2)	295(2)	150(2)	150(2)	150(2)	100(2)	150(2)
Reflections collected	40368	20601	13209	19971	11424	19668	19694
Independent reflections (R_{int})	11227(0.0588)	10708(0.0531)	9463(0.0211)	10444(0.0246)	5128(0.0152)	10293(0.0140)	10268(0.0577)
Data/Parameters	11227/388	10708/388	9463/388	10444/472	5128/388	10293/496	10268/388
GOF on F^2	0.941	0.861	1.083	1.096	1.004	1.272	1.035
R_1 [$I \geq 2\sigma(I)$]	0.0521	0.0342	0.0399	0.0276	0.0193	0.0209	0.0291
wR_2	0.1190	0.0666	0.0954	0.0660	0.0559	0.0544	0.0725

Table 4. Selected bond length, distance between Ln^{3+} and K^{+}, and tropolone rings with π-π interactions in isolated complexes.

Complex	Tb	Dy	Ho	Er	Tm	Yb	Lu
Ln-O(Å)	2.37(1)	2.35(2)	2.34(2)	2.34(2)	2.32(2)	2.31(2)	2.32(2)
K-O(μ) (Å)	2.796	2.811	2.788	2.795	2.803	2.774	2.779
K-O(C=O) (Å)	2.784(5)	2.656(3)	2.651(4)	2.659(2)	2.650(3)	2.6464(17)	2.643(2)
Ln-Ln(Å)	7.251	7.3048(5)	7.2622(4)	7.2758(10)	7.296(3)	7.2409(3)	7.2465(4)
K-K(Å)	7.244	7.3048(5)	7.2622(4)	7.2758(10)	7.296(3)	7.2409(3)	7.2465(4)
Ln-K(Å)	3.8935(10)	3.8875(6)	3.8760(7)	3.8693(7)	3.8736(15)	3.8470(4)	3.8496(5)
Ln-K'(Å)	3.9273(10)	3.8954(6)	3.8603(7)	3.8813(6)	3.8933(13)	3.8593(4)	3.8630(5)
Distance 1(Å)[a]		3.30	3.29	3.26	3.29	3.23	3.23
Distance 2(Å)[a]		3.68	3.70	3.66	3.70	3.64	3.63

a. For π-π interaction (see following text)

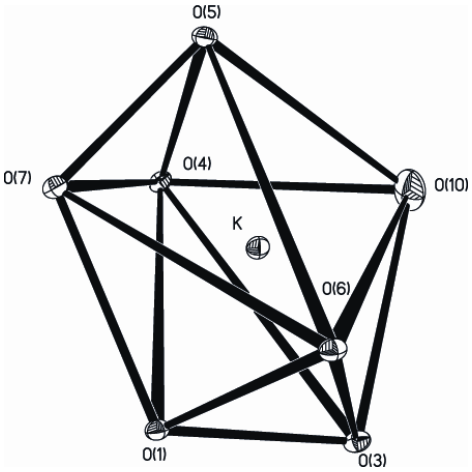

Figure 15. Coordination polyhedron of K in $\{K[Yb(Trop)_4]DMF\}_{\infty}$.

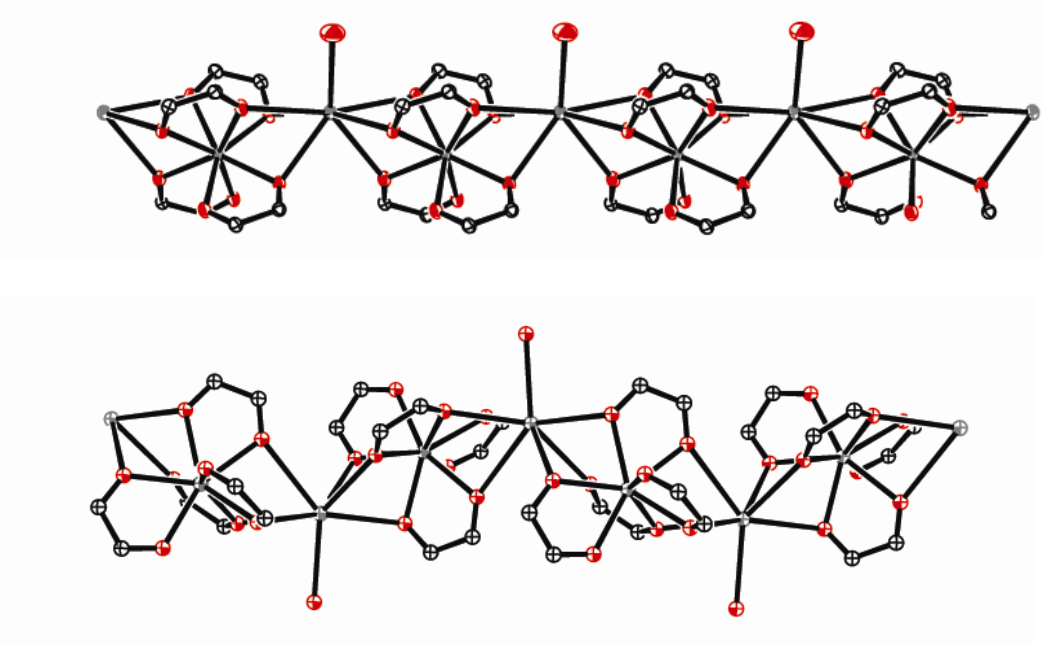

Figure 16. Polymeric chain in $\{K[Yb(Trop)_4]DMF\}_{\infty}$ (up) and $[K(TbL_4)DMF]_{\infty}$ (bottom).

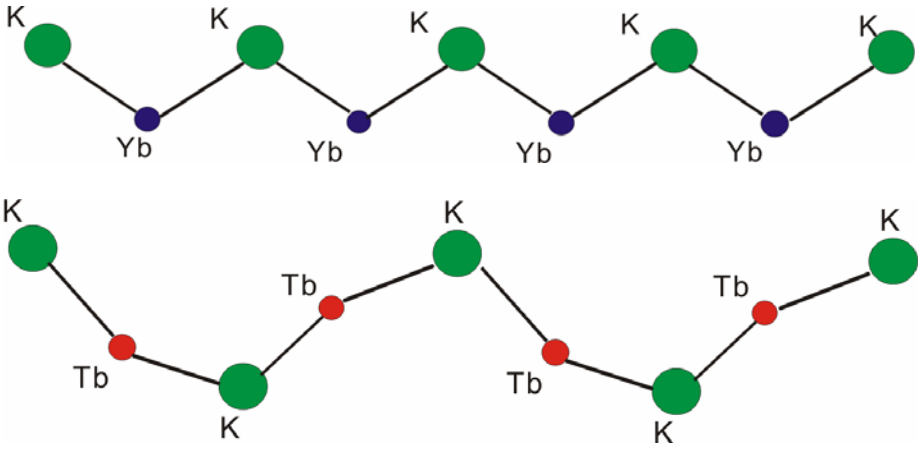

Figure 17. Simplified polymeric chain in $\{K[Yb(Trop)_4]DMF\}_\infty$ (up, Ln = Yb, bottom, Ln = Tb).

Hydrogen bonds

Although C-H•••O hydrogen bonds are weak hydrogen bonds (<12 kJ·mol-1), they play a very important role in supramolecular chemistry and crystal engineering.[63] C–H•••O hydrogen bonds were identified and the data are listed in Table 5. The distances and angles between the donor and accepter atoms are all in the range of typical C-H•••O hydrogen bonds.[64] Figure 18 shows the hydrogen bonds in Yb and Tb complexes.

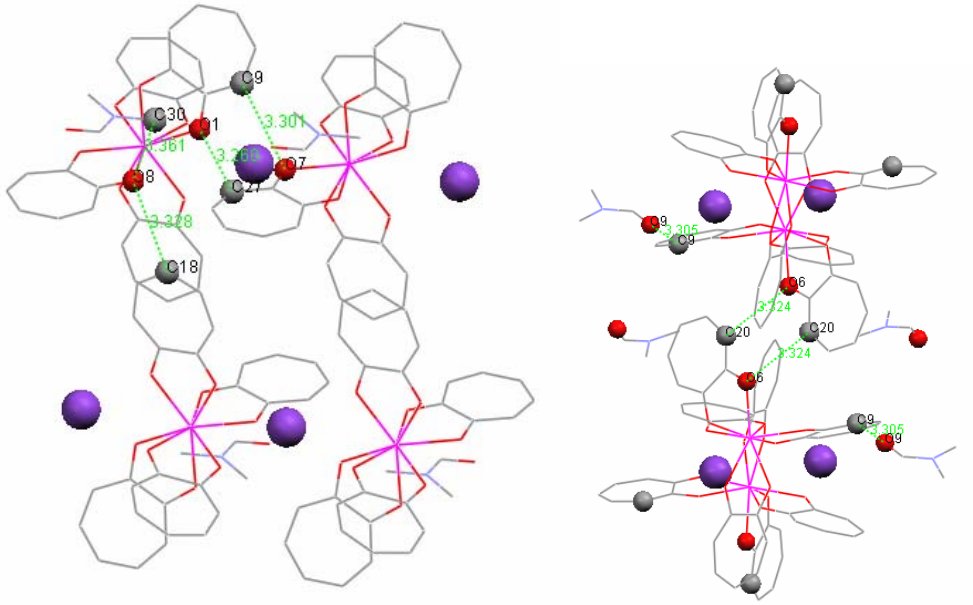

Figure 18. View of C–H•••O hydrogen bonds in $[K(YbL_4)DMF]_\infty$ (left) and $[K(TbL_4)DMF]_\infty$ (right) (grey: C, red: O, blue: N, pink: Ln, purple: K).

π-π stacking

π-π stacking interaction is one of the noncovalent interactions in supramolecular chemistry. There are typically two types: face-to face and slipped (Figure 19).

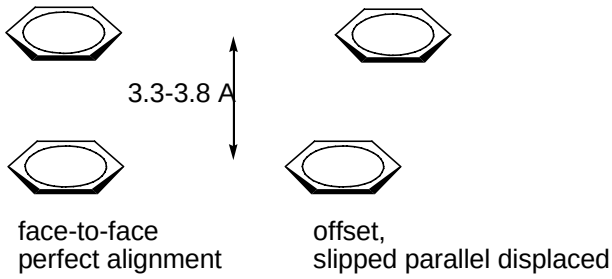

Figure 19. Two types of orientations of π-π stacking

Although no π-π interaction was found in Tb complex, two π-π interactions were identified in each of the other six complexes. In the Ho complex, the distance between the tropolone rings (C8-C14) in adjacent polymeric chains are 3.293 Å. The distance between the rings (C15-C21) is 3.695 Å. (Figure 20). Because the planes are crystallographic identical, the dihedral angles are zero. The distance values are listed in Table 4.

Geometry analysis of the complexes

For eight coordination geometry, there are two main kinds of coordination polyhedrons: square antiprism (D_{4d}) and dodecahedron (D_{2d}). Kepert has a good review of the aspects of the stereochemistry of eight-coordination.[65] The coordination polyhedron around lanthanide ion in $[Ln(trop)_4]^-$ is best described as a distorted dodectahedron (D_{2d}) (Figure 21). Typical dodecahedron model is shown in Figure 22. For tetra-bidentate coordination complexes, value *b*, ratio between bond length of M-L and the distance of the two atoms in bidentate ligands, can be used as criteria to differentiate square antiprism and dodecahedron. If *b* is less than 1.1, the compounds generally have the D_{2d} dodectahedral structure. As *b* is increased, the structure will be

distorted. When *b* is increased to 1.15-1.20, the complexes are best described as intermediate with D_2 stereochemistry. When the *b* value reaches 1.30, the complexes have typical D_4 square antiprism structure. The *b* value for the tropolone lanthanide complexes are shown in Table 7, and are between 1.07 and 1.10, therefore the geometry of the polyhedron can be best described as dodecahedron.

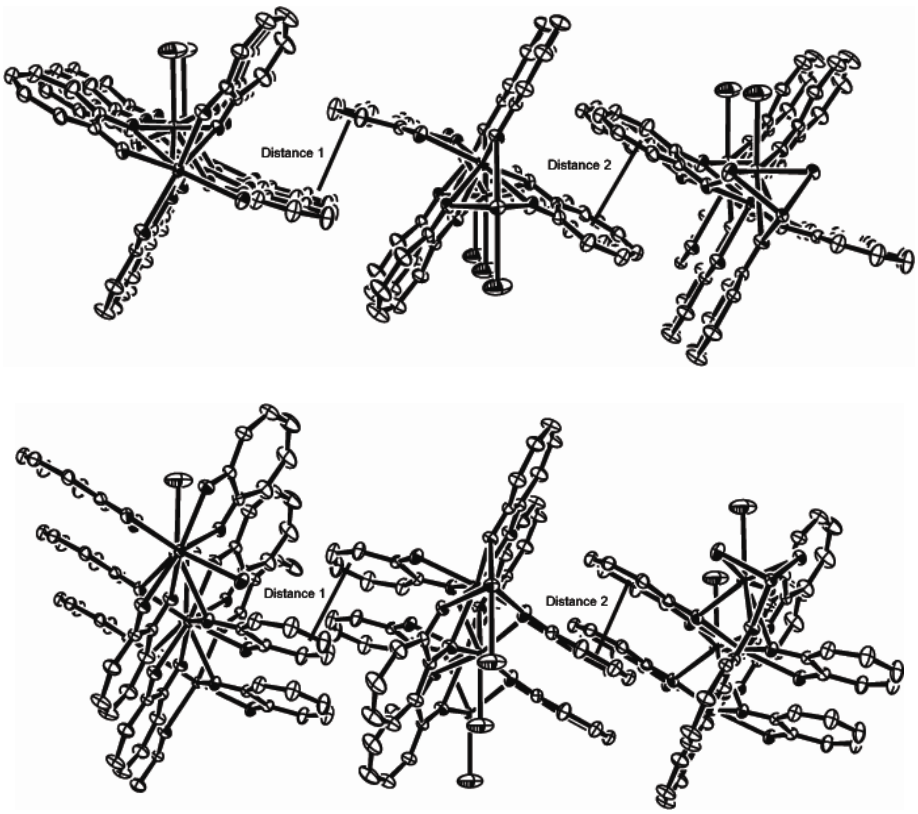

Figure 20. Two different views of π-π interaction in $\{K[Yb(Trop)_4]DMF\}_\infty$.

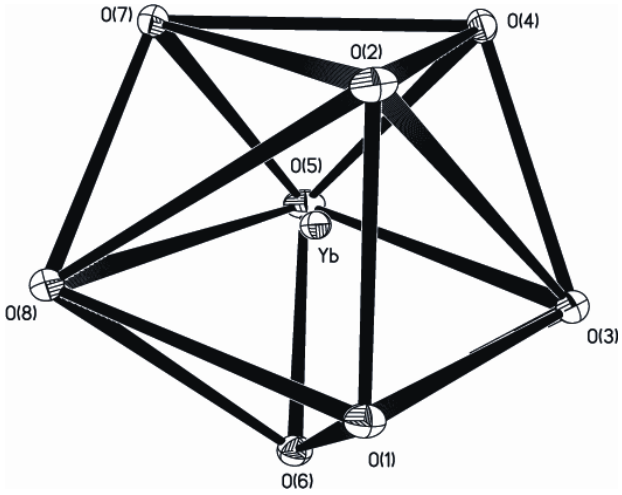

Figure 21. Coordination polyhedron around Yb^{3+} in $[Yb(Trop)_4]^-$.

Table 5. Hydrogen bonds data in the complexes.

	Donor–H•••Acceptor	Distance D–H (Å)	Distance H•••A (Å)	Distance D•••A (Å)	Angle D–H•••A (°)
Tb	C(9)–H(9A)•••O(9)	0.93	2.47	3.306	149
	C(20)–H(20A)•••O(6)[a]	0.93	2.47	3.324	153
	Symmetry code: a = 1-*x*, 1-*y*, 1-*z*				
Dy	C(2)–H(2A)•••O(6)[a]	0.93	2.47	3.327	153
	C(26)–H(26A)•••O(1)[b]	0.93	2.51	3.372	155
	C(42)–H(42A)•••O(9)	0.96	2.32	2.753	107
	C(43)–H(43B)•••O(2)[c]	0.96	2.57	3.460	154
	Symmetry codes: a = -1+*x*, *y*, *z*; b = 1+*x*, *y*, *z*; c = *x*, -1+*y*, *z*				
Ho	C(9)–H(9A)•••O(7)[a]	0.95	2.44	3.326	155
	C(18)–H(18A)•••O(8)[b]	0.95	2.51	3.338	145
	C(27)–H(27A)•••O(1)[c]	0.95	2.40	3.274	152
	C(32)–H(32A)•••O(10)	0.98	2.35	2.773	105
	C(33)–H(33C)•••O(8)[d]	0.98	2.50	3.381	150
	Symmetry codes: a = 1+*x*, *y*, *z*; b = 1-*x*, 1-*y*, -*z*; c = -1+*x*, *y*, *z*; d = 1+*x*, -1+*y*, *z*				
Er	C(9)–H(9A)•••O(7)[a]	0.92	2.46	3.331	158
	C(18)–H(18A)•••O(8)[b]	0.89	2.58	3.362	147
	C(27)–H(27A)•••O(1)[c]	0.91	2.42	3.285	158
	C(32)–H(32A)•••O(10)	0.98	2.36	2.785	106
	C(33)–H(33C)•••O(8)[d]	0.98	2.50	3.389	151
	Symmetry codes: a = 1+*x*, *y*, *z*; b = 1-*x*, 1-*y*, -*z*; c = -1+*x*, *y*, *z*; d = 1+*x*, -1+*y*, *z*				
Tm	C(12)–H(12A)•••O(6)[a]	0.95	2.47	3.339	156
	C(26)–H(26A)•••O(3)[b]	0.95	2.45	3.322	153
	C(42)–H(42A)•••O(5)[c]	0.98	2.55	3.453	153
	C(43)–H(43A)•••O(9)	0.98	2.36	2.783	106
	Symmetry codes: a = -1+*x*, *y*, *z*; b = 1+*x*, *y*, *z*; c = -1+*x*, 1+*y*, *z*				
Yb	C(9)–H(9)•••O(7)[a]	0.94	2.40	3.3012	160
	C(18)–H(18)•••O(8)[b]	0.92	2.52	3.3285	146
	C(27)–H(27)•••O(1)[c]	0.98	2.34	3.2596	156
	C(30)–H(8A)•••O(8)[d]	1.03	2.44	3.3605	149
	Symmetry codes: a = 1+*x*, *y*, *z*; b = 1-*x*, 1-*y*, -*z*; c = -1+*x*, *y*, *z*; d = 1+*x*, -1+*y*, *z*				
Lu	C(2)–H(2A)•••O(6)[a]	0.95	2.39	3.2605	153
	C(26)–H(26A)•••O(1)[b]	0.95	2.41	3.2987	156
	C(34)–H(34A)•••O(2)[c]	0.95	2.52	3.3282	144
	C(42)–H(42A)•••O(9)	0.98	2.36	2.7891	105
	C(43)–H(43B)•••O(2)[d]	0.98	2.47	3.3589	150
	Symmetry codes: a = -1+*x*, *y*, *z*; b = 1+*x*, *y*, *z*; c = 1-*x*, 1-*y*, -*z*; d = *x*, -1+*y*, *z*				

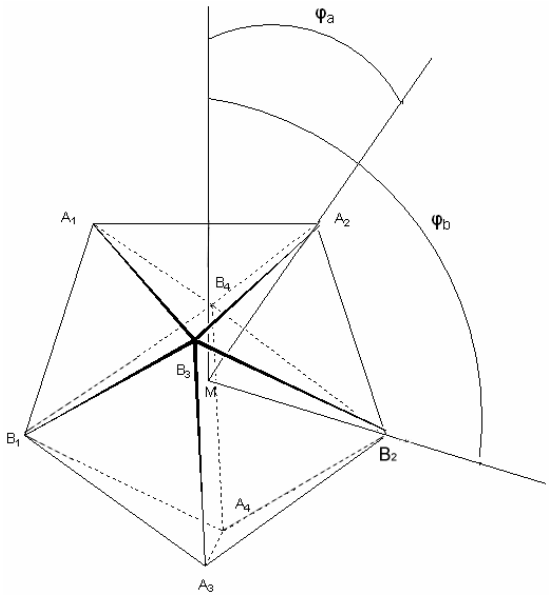

Figure 22. Dodecahedron model for the geometrical analysis.

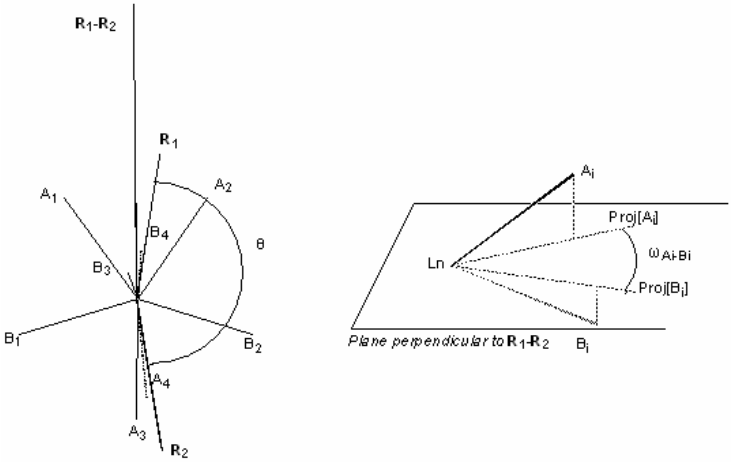

Figure 23. Definition of the angles and vectors used in the geometrical analysis.

Table 6. Definition of atoms in the geometrical analysis.

	Tb	Dy	Ho	Er	Tm	Yb	Lu
A_1	O5	O6	O7	O7	O3	O7	O6
B_1	O6	O5	O8	O8	O4	O8	O5
A_2	O7	O8	O4	O4	O8	O4	O8
B_2	O8	O7	O3	O3	O7	O3	O7
A_3	O2	O4	O2	O1	O2	O1	O4
B_3	O1	O3	O1	O2	O1	O2	O3
A_4	O3	O1	O5	O6	O6	O6	O1
B_4	O4	O2	O6	O5	O5	O5	O2

As discussed above, the eight coordination polyhedron in the tropolone complexes is best described as distorted dodecahedron. To quantify the distortion, coordination sphere around Ln(III) has been investigated using a geometrical analysis assuming that the S_4 symmetry is maintained (Figure 23). Three parameters are needed to confirm the dodecahedral shape: the angle between the $\mathbf{R_{M\text{-}A}}$ (Vector of M-A bond) and the s_4 axis (φ_a), the angle between the $\mathbf{R_{M\text{-}B}}$ (Vector of M-B bond) and the s_4 axis (φ_b), and the ratio a, between bond length |M-A| / |M-B|. For an ideal dodecahedron, these three values are 35.2°, 106.5° and 1.03 respectively. For a dodecahedron hard sphere model, these values are 36.9°, 110.5° and 1.00 respectively. To determine the pseudo-s_4 axis, the sum of vectors M-A_1, M-A_2, M-B_3 and M-B_4 was defined as vector $\mathbf{R_1}$; the sum of vectors M-B_1, M-B_2, M-A_3 and M-A_4 was defined as vector $\mathbf{R_2}$; and the vector $\mathbf{R_1\text{-}R_2}$ is defined as the pseudo s_4 axis (Figure 23). The projections of Ln and the eight oxygen atoms of the coordination sphere onto a plane perpendicular to the $\mathbf{R_1\text{-}R_2}$ direction were then calculated. The angle ω_i between the vectors Ln-O belonging to the same ligand ($\mathbf{Ln\text{-}A_i}$ and $\mathbf{Ln\text{-}B_i}$) show the deformation of the pseudo-dodecahedron from an ideal dodecahedron (ideal $\omega = 0°$). The assignments for oxygen atom in different complexes are shown in Table 6. The values for φ, θ, and ω_i are reported in Table 7.

The Cambridge Structure Database (CSD) was searched for similar tropolone eight coordinated ML_4 complexes, and six similar structures have been reported. Similar calculations were carried out for these complexes and the data is listed in Table 7.

Table 7. Results of geometrical analysis of dodecahedra in complexes.

	Tb	Dy	Ho	Er	Tm	Yb	Lu	Zr[66]	Nb[67]	Hf[68]	Sn[69]	Sc1[70]	Sc2[71]
φ_a (°)[1]	36.48	39.15	39.12	39.02	38.85	38.98	38.89	36.78	35.72	36.02	35.72	36.34	36.44
φ_b (°)[1]	101.36	104.54	105.07	105.14	105.10	105.65	105.33	105.28	106.23	105.60	106.74	104.70	104.66
a[2]	1.00	0.99	1.00	0.99	0.99	0.99	0.99	1.01	1.00	1.00	1.01	1.00	1.00
θ (°)[3]	177.58	172.40	172.33	172.51	173.16	173.03	172.79	172.83	178.21	179.02	178.21	171.61	171.73
ω_i (°)[4]	0.43	2.97	3.26	2.91	9.45	21.34	3.23	0.88	4.18	2.08	5.96	18.18	9.16
	2.56	0.82	1.38	1.43	2.56	9.67	1.60	2.06	4.70	4.63	6.76	11.09	15.20
	5.75	7.34	17.48	5.06	2.57	2.18	5.83	3.11	10.43	2.21	20.06	5.54	5.88
	3.47	18.89	5.79	3.35	5.31	0.91	12.00	0.77	9.73	2.58	18.70	8.08	8.70
b[5]	1.07	1.08	1.09	1.09	1.10	1.10	1.10	1.12	1.16	1.14	1.17	1.13	1.13

1. φ_a and φ_b are the average values of the angles between $\mathbf{R_1}$-$\mathbf{R_2}$ and A_i (i = 1, 2, 3, 4) and B_i (i = 1,2 3,4) respectively.
2. *a* is the ratio of bond length |M-A| to |M-B|
3. θ is the angle between $\mathbf{R_1}$ and $\mathbf{R_2}$
4. ω_i are the angle between the vectors **Ln-O** belonging to one same tropolone ligand
5. *b* is the ratio between bond length of M-L and the distance of the two oxygen atoms in bidentate ligands

It can be seen from the data that the geometries for the tropolone lanthanide complexes have some distortion from the ideal dodecahedron. Compared to other tropolone non-lanthanide ML_4 complexes, this distortion is large. We attribute this to the effect of K^+ and the DMF molecule. K^+ is coordinated to the oxygen atoms in the tropolone ligands, and the DMF is coordinated with K^+. This makes one of the tropolone planes deviate from the ideal position and, as a consequence, two of the four dihedral angles change from the ideal values of 90°. One of the dihedral angles is larger and the other one is smaller (Table 8).

Table 8. Dihedral angles between four tropolone planes in complexes.

	Tb	Dy	Ho	Er	Tm	Yb	Lu
Angle 1(°)	105.159	92.549	91.978	92.359	92.744	92.371	92.306
Angle 2(°)	79.660	102.434	103.966	103.595	102.691	102.691	103.878
Angle 3(°)	95.757	73.701	72.182	72.459	73.533	73.533	72.360
Angle 4(°)	88.207	88.659	89.268	89.018	88.402	88.402	88.875

Structure comparison with lanthanide complex with 1-hydroxy-2-pyridinone

Picard *et al.*[72] recently reported the crystal structure of lanthanide complexes with 1-hydroxy-2-pyridinone (HOPO) as shown in Figure 24. HOPO is a cyclic hydroxamic acid, which can be used as a bidentate ligand. It is very similar to tropolone in structure, except it is six-membered ring. They prepared ML_4 complexes of Eu and Gd with HOPO.

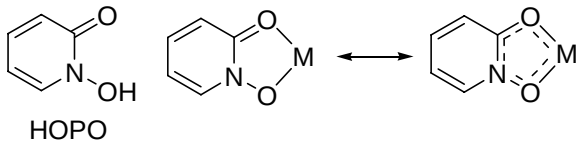

Figure 24. Structure of HOPO ligand and its coordination mode with metal ion.

The structure of Eu complex with HOPO is shown in Figure 25. There are two different Eu ions in the asymmetric unit. Four HOPO ligands are coordinated to each

Eu ion, and the coordination number is eight. Using the formula mentions before, The *b* value can be calculated to be 1.09, which indicates that the coordination polyhedron is also best described as a dodecahedron. Na^+ was used as the counter ion instead of K^+. Both of the Na^+ ions are six coordinate. Na(1) is coordinated with five oxygen atoms from HOPO, one from water. Na(2) is coordinated with four oxygen atoms, and the other two from water. The distance between two Eu ions is 7.046 Å, which is shorter than the typical distance observed in tropolone complexes (about 7.26 Å), partly due to the smaller size of Na. According to Shannon's radii, six coordinated Na is 1.16 Å, seven coordinated K is 1.60 Å.[73]

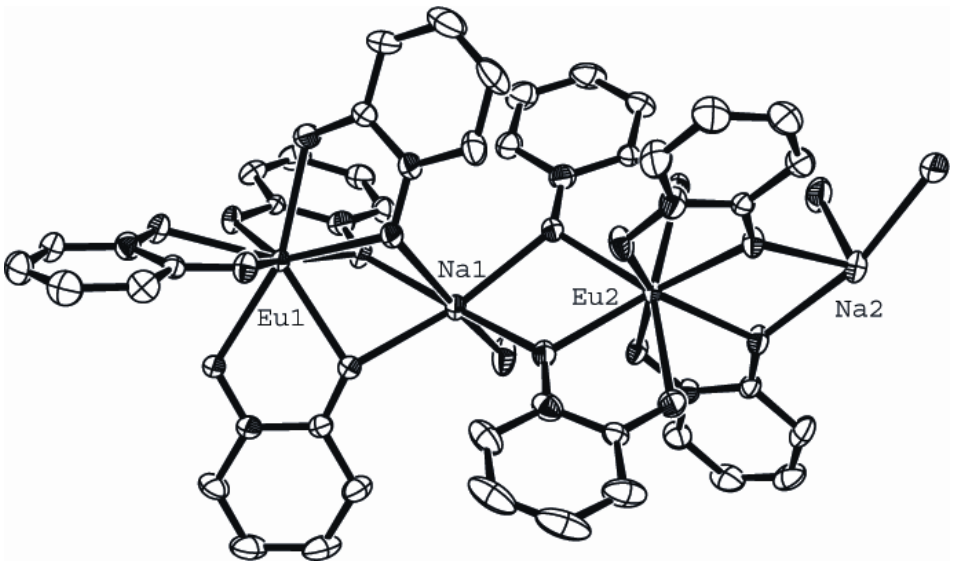

Figure 25. Structure of Eu complex formed with HOPO ligand[72].

The average bite angles, (angle of O-M-O in bidentate ligand) are 65.7º and 66.0º for HOPO complex with Eu and Gd respectively. These values are not very different with the bite angle in tropolone complexes (65.1º-67.0º). So the effect of seven membered ring on the bite angle is very limited. As far as coordination mode is concerned, there are two types of coordination in both complexes of tropolone and HOPO (Figure 26) for O atoms. The first type is the ligand coordinates with the Ln cation, and two alkaline cations. The other only coordinates with one Ln cation and

one alkaline cation. In the crystal structure of tropolone complexes, for one ML_4 unit, two of them are of type *a*, the other two are of type *b* (Figure 14). In the HOPO complexes, for one $(ML_4)_2$ unit, only one ligand has the type *a* coordination mode (Figure 25).

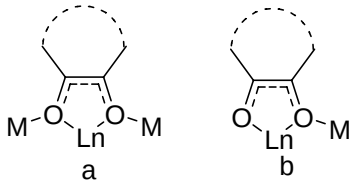

Figure 26. Coordination modes in the complexes.

2.4.3 Solution study

2.3.2.1 Spectrophotometric titration

To determine the number, nature of species formed in solution and the corresponding stability constants for the lanthanide tropolone complexes, spectrophotometric titrations were performed for La, Nd, Gd, and Yb. Spectra were collected varying the M:L ratio in DMSO. Typical example of titration for Yb complex is shown in Figure 27a. Software SPECFIT[74] was used to treat the experimental data. Factor analysis indicated that there are five independent colored species in the solution (Figure 27b-14d). Experimental data were fitted with a mode where four types of complexes: ML, ML_2, ML_3 and ML_4 are formed successively. Stability constants were obtained with this model (Table 9). Based on the stability constants, the experimental concentration needed to maintain the main species of the complex (at least 80%), ML_4, in solution during the photophysical study was calculated to be $>5\cdot10^{-5}$ mol/L.

Table 9. Overall formation constants for tropolone complexes $Ln(trop)_n$ and stepwise formation constant K_n.

Species		La	Nd	Gd	Yb
$[Ln(trop)]^{2+}$	$\log\beta_1$	8.58±0.2	6.41±0.2	6.70±0.2	6.70±0.2
$[Ln(trop)_2]^{+}$	$\log\beta_2$	14.75±0.3	12.25±0.2	12.60±0.2	13.11±0.2
$[Ln(trop)_3]$	$\log\beta_3$	19.95±0.3	17.58±0.3	18.31±0.2	19.12±0.2
$[Ln(trop)_4]^{-}$	$\log\beta_4$	24.58±0.2	23.28±0.3	23.26±0.2	24.42±0.2
	$\log K_1$	8.58	6.41	6.70	6.70
	$\log K_2$	6.17	5.84	5.90	6.41
	$\log K_3$	5.20	5.33	5.71	6.01
	$\log K_4$	4.63	5.70	4.95	5.30

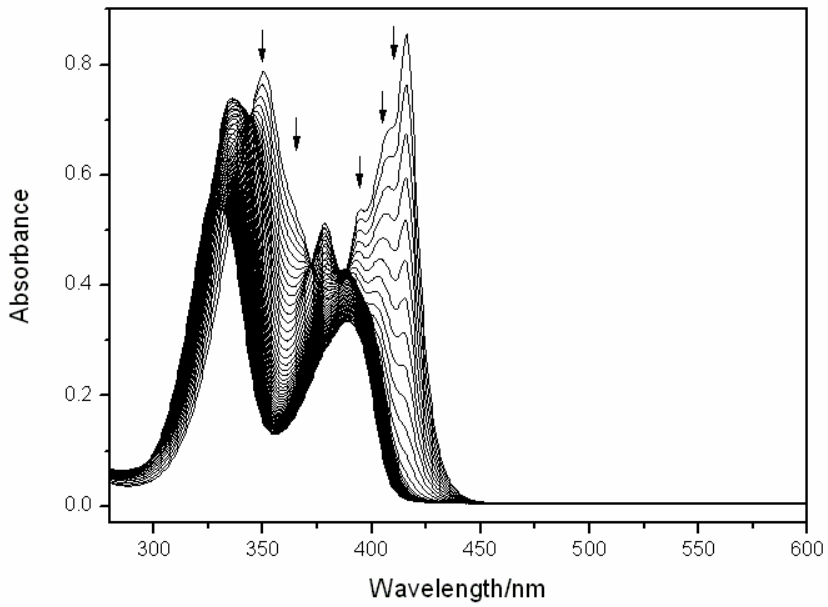

Figure 27a.

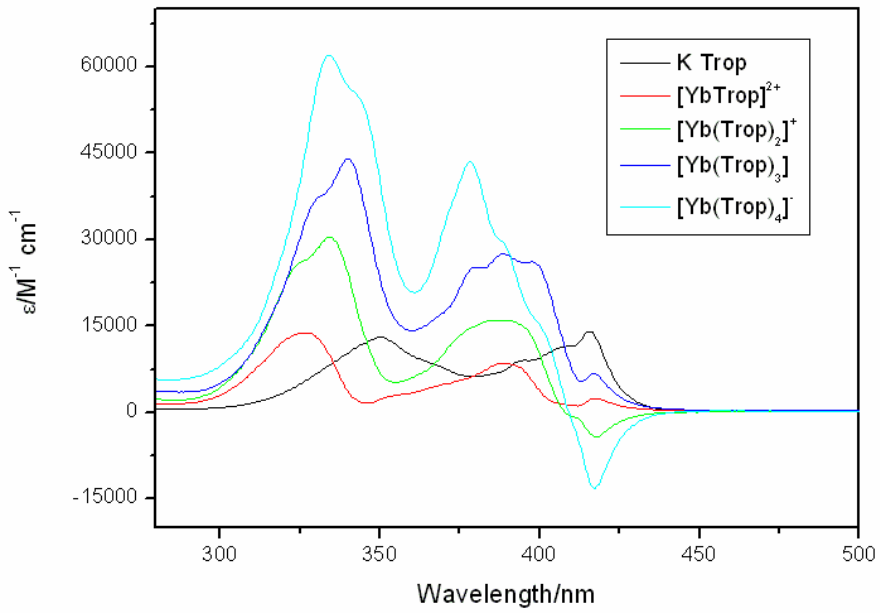

Figure 27b

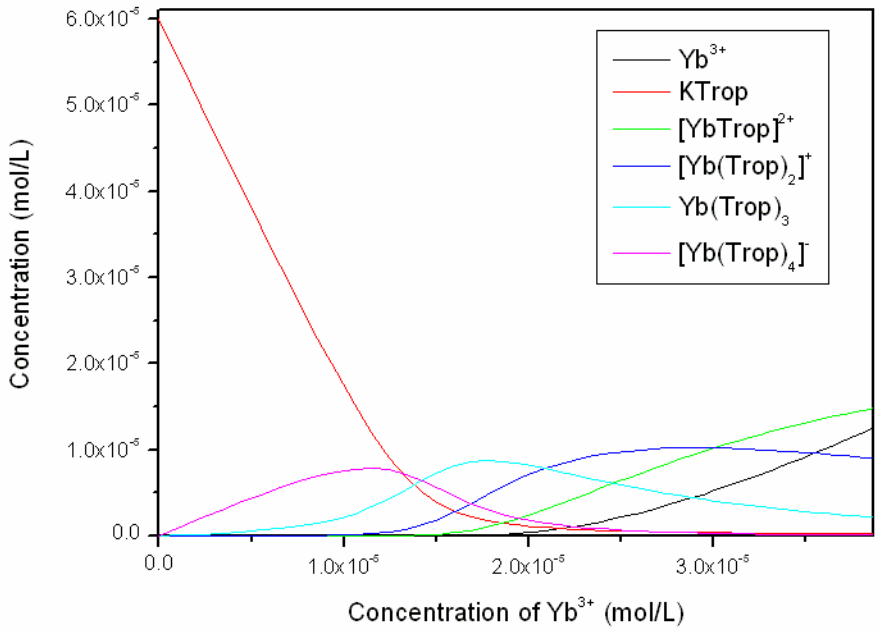

Figure 27c

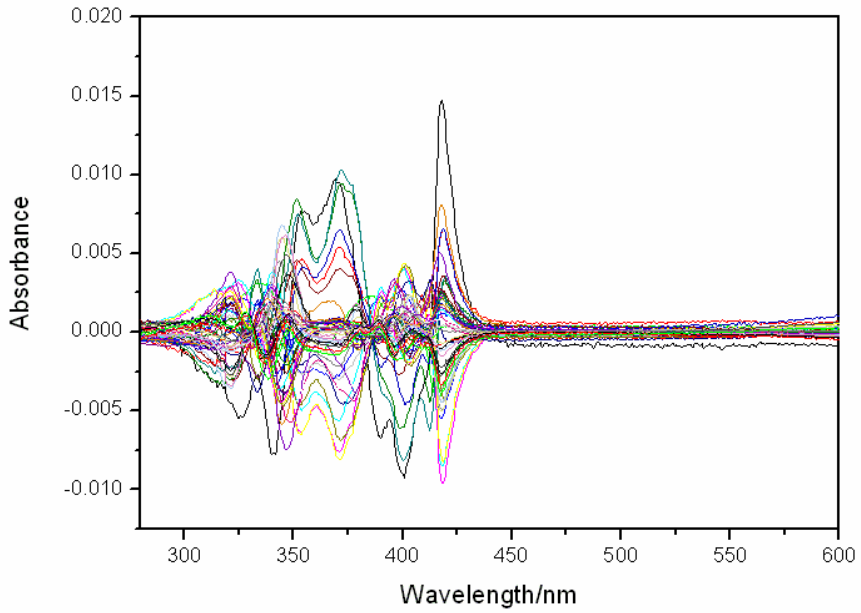

Figure 27d.

Figure 27. Results of spectrophotometric titration of KTrop with Yb^{3+} (a. Experimental spectra; b. Calculated spectra for the five colored species; c. Distribution of different species versus metal concentration; d. Residuals from the calculation).

2.3.2.2 NMR study

The ^{1}H NMR spectra of tropolone, potassium tropolonate, and the diamagnetic Lu^{3+} complex $K[Lu(Trop)_4]$ were measured in d_6-DMSO. The chemical shift data are given in Table 10 and the ^{1}H NMR are spectra shown in Figure 28.

Due to the strong intramolecular hydrogen bonds in tropolone, the proton in the OH group has a broad band with a chemical shift of 10.2 ppm. After deprotonation, all the ring-protons in the tropolone shift to higher field. This is not easily explained, although the same effect was observed by Poh.[75] When coordinated with Lu^{3+}, proton signals are shifted back to lower field because of the electrowithdrawing effect of Lu^{3+}, which decreases the electronic density on the protons.

Table 10. ^{1}H NMR data for the ligand and complex in d_6- DMSO (d, doublet; t, triplet).

Compounds	δ_{H3}	δ_{H1}	δ_{H2}
$C_7H_6O_2$	7.04 (t)	7.22 (d)	7.41 (dd)
$C_7H_5O_2K$	6.02 (t)	6.35 (d)	6.73 (dd)
$C_{28}H_{20}O_8KLu$	6.68 (t)	6.86 (d)	7.25 (dd)

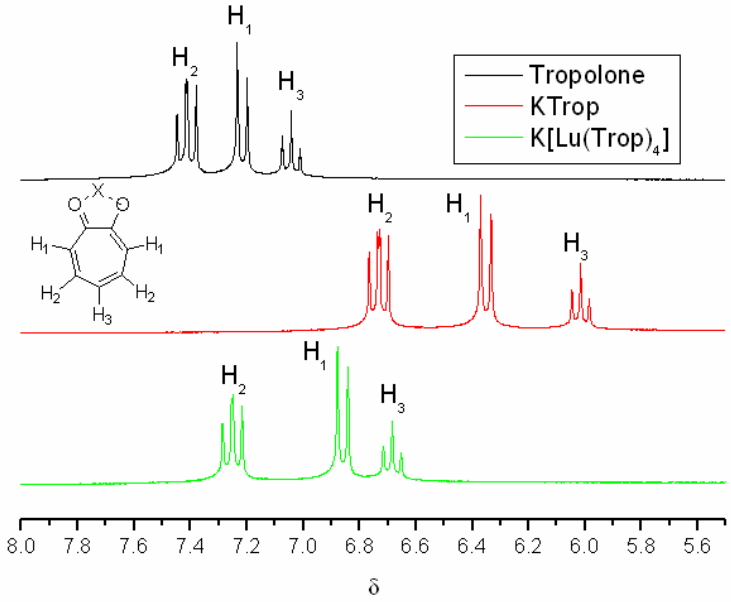

Figure 28. ^{1}H NMR spectra of tropolone, potassium tropolonate and Lu complex at 298 K in d_6-DMSO.

2.3.2.3 ESI-MS

Electrospray ionization mass spectra (ESI-MS) were performed with all the lanthanide complexes in a mixture of DMF and methanol solution. The data are listed in Table 11. Selected spectra for different species in complexes are shown in Figures 29a-29g. For the negative ion spectra, the highest abundant $(LnL_4)^-$ peaks are observed for all the complexes, which indicates the formation of ML_4 complex in solution. In addition, the Trop anion was also detected, with lower abundance, which is due to the partial dissociation of the complex in the experimental conditions. For the positive ion spectra, several types of ions were observed: $(LnL_2)^+$, $(LnL_2+DMF)^+$, $(LnL_3+Na)^+$, $(LnL_3+K)^+$, $(LnL_4+2Na)^+$, $(LnL_4+Na+K)^+$, $(LnL_4+2K)^+$, $(Ln_2L_5)^+$, $(Ln_2Ln_6+Na)^+$,

$(Ln_2Ln_6+K)^+$, $(L_3Ln_8)^+$, $(Ln_3L_9+Na)^+$, $(Ln_3L_9+K)^+$. The presence of the di- and trinuclear species indicates that there is significant interaction between the LnL_n units, in the experimental conditions (Approx. Concentration of complexes: 10^{-2}-10^{-3} mol/L). This is an indication that the polymeric structure found in the solid state partially remains in solution. Picard *et al.*[72] also observed this polynuclear pattern of peaks in ESI-MS with the HOPO complexes tat they have studied. Fragmentation, ligand exchange and clustering reactions during the mass spectral experiments could account for the diverse ionic species observed.

Table 11. The ESI-MS data for lanthanide tropolone complexes.

	$(LnL_2)^+$	$(LnL_2+DMF)^+$	$(LnL_3+Na)^+$	$(LnL_3+K)^+$	$(LnL_4+2Na)^+$	$(LnL_4+Na+K)^+$	$(LnL_4+2K)^+$	$(Ln_2L_5)^+$	$(Ln_2L_6+Na)^+$	$(Ln_2L_6+K)^+$	$(Ln_3L_8)^+$	$(Ln_3L_9+Na)^+$	$(Ln_3L_9+K)^+$	$(LnL4)^-$
La	381	454	525	541			701	883	1027	1043	1385		1545	623
Pr	383	456	527	543			703	887	1031	1047	1391			625
Nd	384	457	530	546			706	893		1053	1400		1560	628
Sm	394	467	538	554		698	714	906	1050	1066	1421		1581	636
Eu	395	468	539	555		699	715	909	1053	1069	1425		1585	637
Gd	400	473	544	560		704	720	921	1065	1081	1441	1585	1601	642
Tb	401	474	545	561		705	721	923	1067	1083	1445		1605	643
Dy	406	479	550	566	694	710	726	931	1075	1091	1457	1601	1617	648
Ho	407	480	551	567	695	711	727	935	1079	1095				649
Er		481	554	570		714	730	939	1083	1099	1470	1614	1630	652
Tm	411	484	555	571				943	1087	1103	1475	1619	1635	653
Yb	416	489	560	576	704	720	736	951	1095	1111	1488	1631	1648	658
Lu	417	490	561	577	705	721	737	955	1099	1115	1493	1637	1653	659
Y	331	404	475	491			651	783	927	943	1235	1379	1395	573

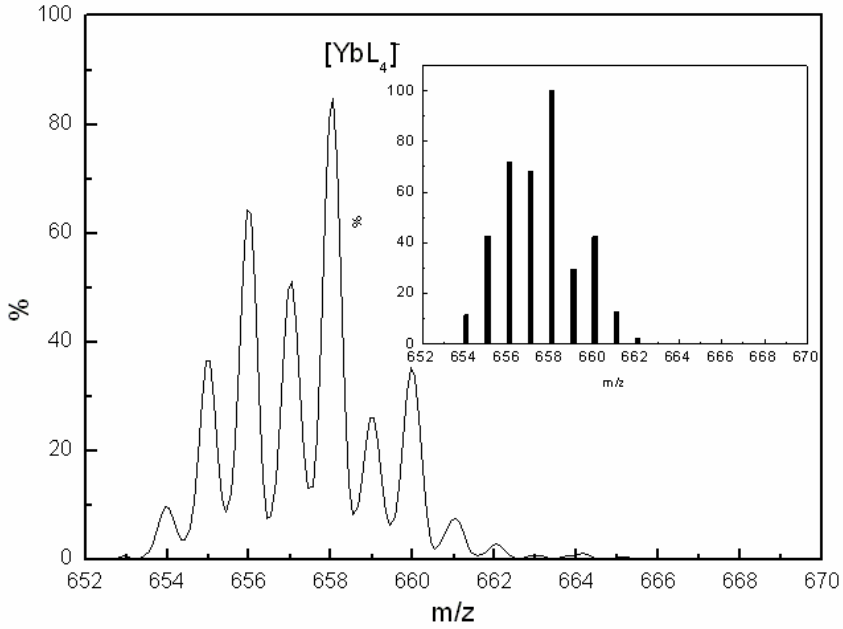

Figure 29a

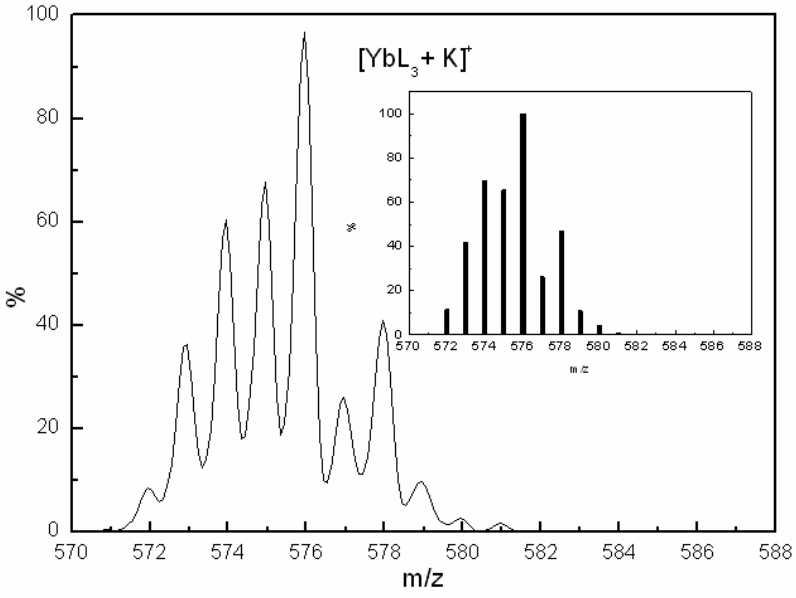

Figure 29b

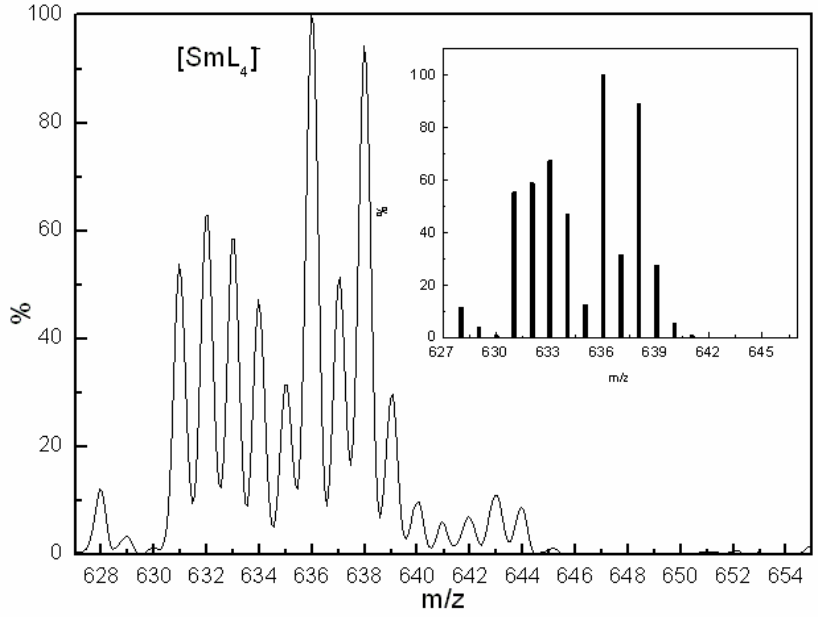

Figure 29c

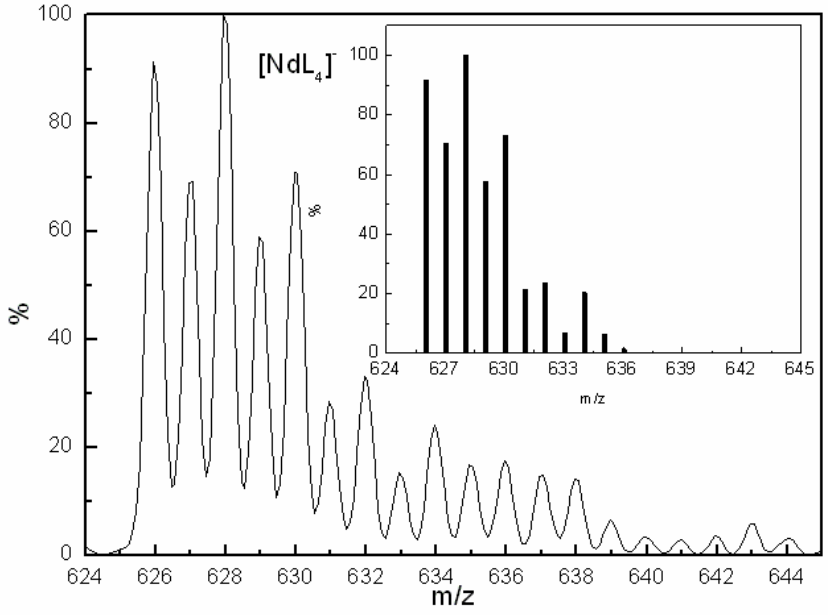

Figure 29d

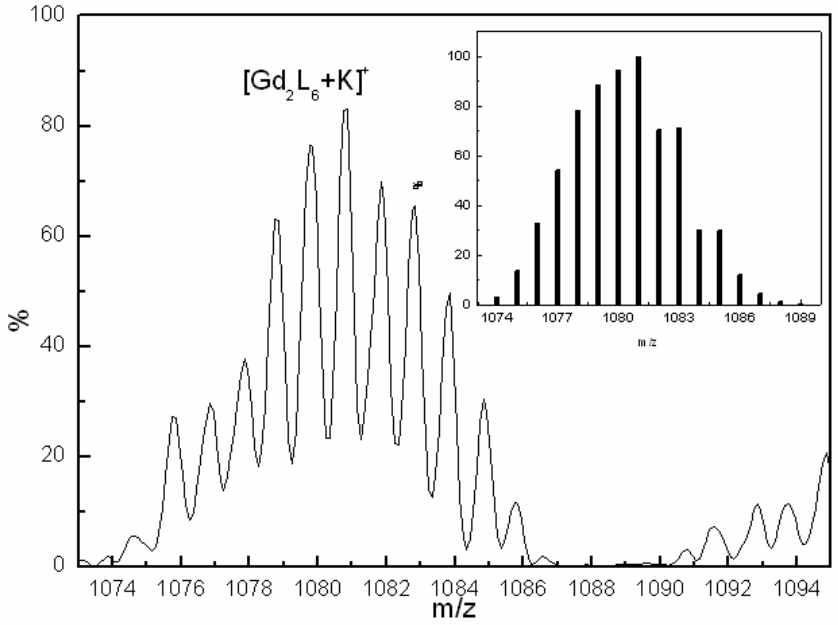

Figure 29e

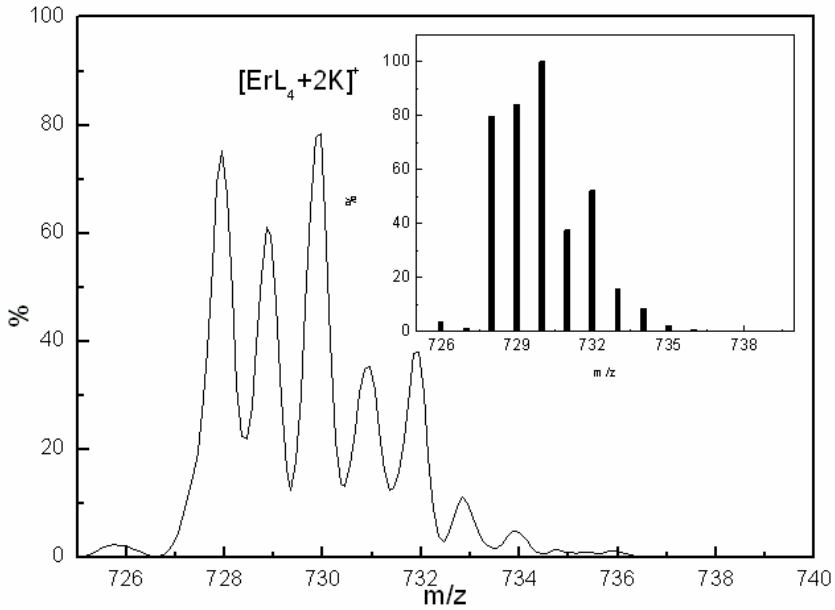

Figure 29f

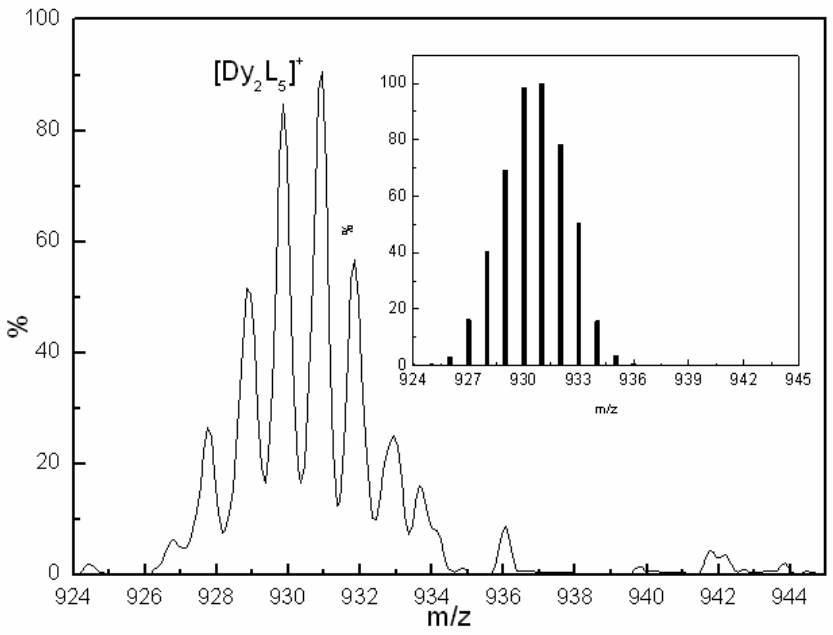

Figure 29g

Figure 29. Selected ESI mass spectra for different species in tropolone lanthanide complexes (Insects are the calculated spectra).

2.4 PHOTOPHYSICAL PROPERTIES

2.4.3 Absorption and excitation spectra

The absorption and excitation spectra of the Yb^{3+} complex are depicted in Figure 30. These spectra are representative for the absorption and excitation spectra of all of the luminescent lanthanide complexes. The resemblance of the excitation spectra with the absorption spectra provides evidence that the metal emission is sensitized by ligand. Also, it can be seen from the spectra that the relative intensity of excitation spectrum from 360 nm to 400 nm is greater than

the absorption over the same range, which indicates that the excitation of the Ln^{3+} through the transition band located lower energy is more efficient.

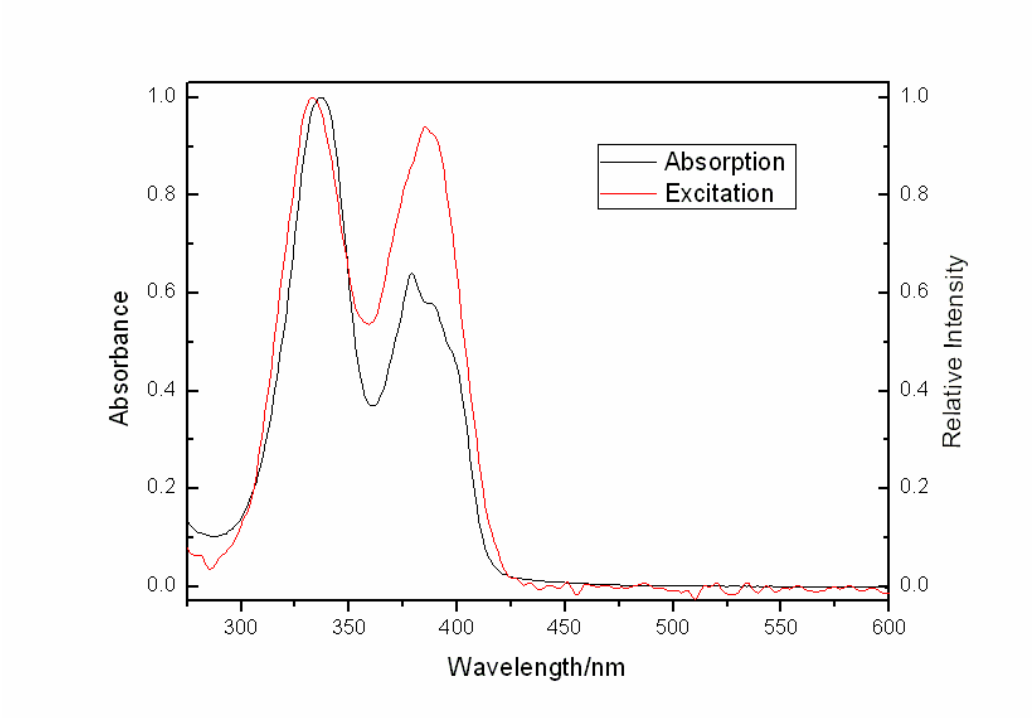

Figure 30. Normalized absorption and excitation spectra of Yb complex (Excitation spectra was obtained by using λ_{em} = 977 nm).

2.4.3 NIR Luminescence

2.4.2.1 Spectra of the Yb^{3+}, Nd^{3+}, Er^{3+}, Ho^{3+} and Tm^{3+} complexes

In the emission spectra (Figure 31), the typical emission bands for Nd^{3+} are located at 897 ($^4F_{3/2} \rightarrow {}^4I_{9/2}$), 1056 ($^4F_{3/2} \rightarrow {}^4I_{11/2}$), and 1331 nm ($^4F_{3/2} \rightarrow {}^4I_{13/2}$). For Er^{3+}, the emission band is 1524 nm ($^4I_{13/2} \rightarrow {}^4I_{15/2}$). Due to the crystal field splitting, there are three maximas in the emission band of the Yb^{3+} complex at 974, 989, and 1023 nm. They are assigned to the $^2F_{5/2} \rightarrow {}^2F_{7/2}$ transition. Besides these three NIR emitting lanthanide complexes, we also observed the NIR luminescence from Ho^{3+} and Tm^{3+} complexes. For Ho^{3+}, three NIR emission bands at 975 ($^5F_5 \rightarrow {}^5I_7$), 1148, 1187 ($^5I_6 \rightarrow {}^5I_8$), and 1479 nm ($^5F_5 \rightarrow {}^5I_6$) were observed. For Tm^{3+} complex, emission bands at 796 nm and 1465 nm are assigned to $^3F_4 \rightarrow {}^3H_6$ and $^3F_4 \rightarrow {}^3H_4$ respectively.

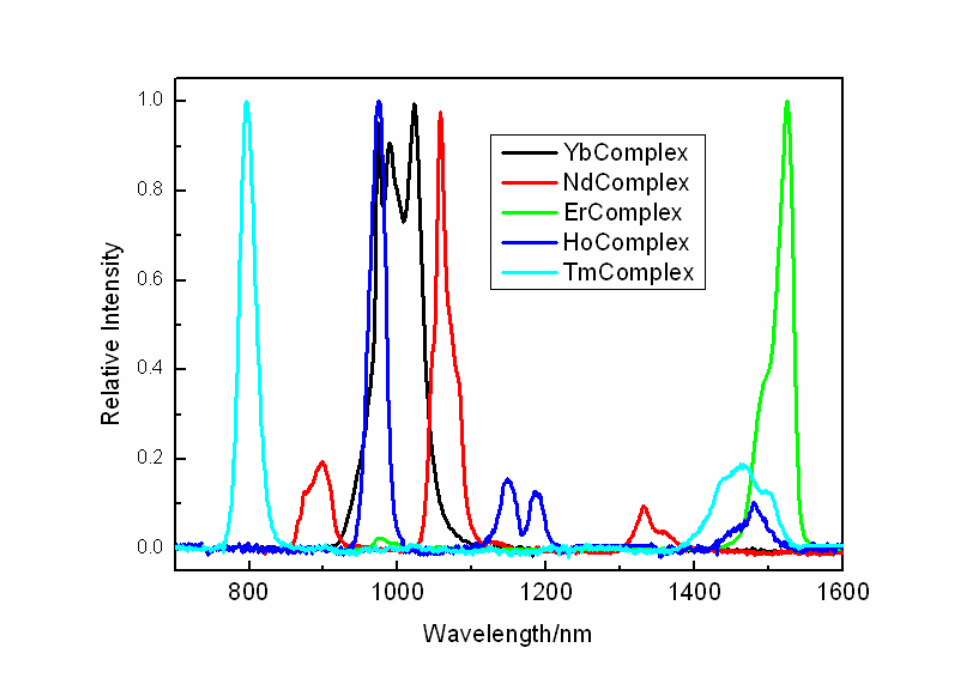

Figure 31. Normalized NIR luminescence spectra of lanthanide complexes.

Ho luminescence has been observed and studied in the solid state (inorganic crystals and glasses). Reisfeld *et al.*[76] studied luminescence of Ho^{3+} in barium zirconium fluoride glass at room temperature. A series of transitions from 383 nm to 991 nm were reported. Recently, van Veggel *et al.*[77] synthesized and studied the luminescent properties of Ho^{3+} doped LaF_3 nanoparticles which are dispersible in organic solvent. They observed two Ho^{3+} NIR transition: $^5F_5 \rightarrow {}^5I_7$ and $^5I_6 \rightarrow {}^5I_8$. More recently, Li *et al.*[78] reported the photoluminescence and electroluminescence of a holmium organic complex in solid film. To our best of knowledge, this is the first observation of a discrete Ho complex's luminescence in non-anhydrous solution. Another characteristic of Ho luminescence is that there is one visible emission band at 651nm ($^5F_5 \rightarrow {}^5I_8$), which can be observed using both VIS and NIR detector in our fluorimeter. (Figure 32)

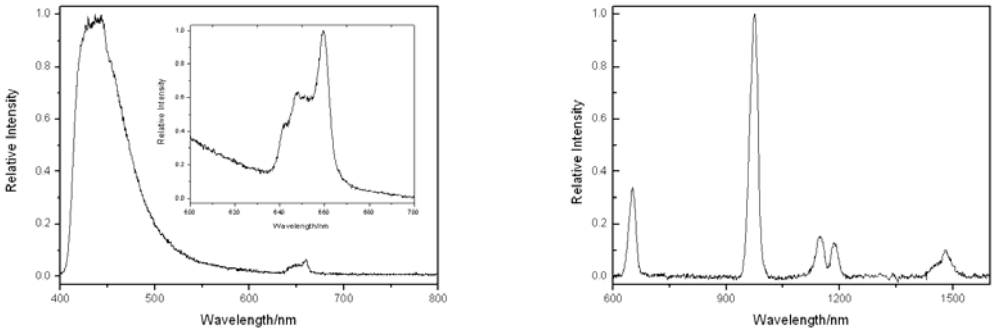

Figure 32. Uncorrected luminescence spectra of Ho tropolone complex (left: measured by VIS detector; right: detected by NIR detector)

In contrast to Ho^{3+}, the luminescence of Tm^{3+} complexes in solution has been described previously. Sharma *et al.*[79] described part of the transitions centered on Tm^{3+} from Tm^{3+} *β*-diketone complexes. Although low in intensity, transition $^3F_4 \rightarrow {}^3H_6$ around 790 nm was observed. Meshkova *et al.*[80] obtained comparable results. Güdel *et al.*[81] studied the high resolution luminescence spectra of Tm complex with 2,6-pyridine-dicarboxylate in single crystals at 15 K. Recently, Li *et al.*[82] reported the electroluminescence of Tm *β*-diketone complex. Two NIR transitions of Tm^{3+} were observed. Our results are consistent with all the former work and we were able to observe more transitions than Schanma in solution.

2.4.2.2 Overall quantum yield

Quantum yield of sensitized emission of $[Ln(Trop)_4]$ in d_6-DMSO and h_6-DMSO were determined by using a Sm complex as a standard[53]. Results are tabulated in Table 12. For the Yb complex, the quantum yields in water and in methanol were also measured.

For the Yb complex, the quantum yield in DMSO is higher than in methanol, which is higher than in water. In all cases, the quantum yields in deuterated solvents are higher than in non-deuterated solvents. This indicates the presence of a non-radiative deactivation process due to the high energy O-H vibration in methanol and water. This deactivation could be due to

quencher's bond in first or second coordination sphere of Ln^{3+} cation, which will be discussed below in detail.

Table 12. Quantum yield for tropolone lanthanide complexes in various solvents.

Complex	Solvent	deuterated		non-deuterated		$k_{q,\ solv}$ (s^{-1})
		QY	Lifetime (μs)	QY	Lifetime (μs)	
	DMSO	$2.2\cdot10^{-2}$(3)	18.13(6)	$1.9\cdot10^{-2}$(1)	12.43(9)	$2.53\cdot10^{4}$
Yb	Methanol	$1.6\cdot10^{-2}$(2)	13.02(1)	$1.3\cdot10^{-3}$(2)	1.62(3)	$5.40\cdot10^{5}$
	Water	$7.4\cdot10^{-3}$(1)	10.03(6)	$2.4\cdot10^{-4}$(3)	0.75(1)	$1.23\cdot10^{6}$
Nd[a]	DMSO	$3.6\cdot10^{-3}$(7)	1.65(1)	$2.1\cdot10^{-3}$(1)	1.10(4)	$3.03\cdot10^{5}$
Er[a]	DMSO	$3.2\cdot10^{-4}$(4)		$1.7\cdot10^{-4}$(1)		
Tm[b]	DMSO	$5.7\cdot10^{-5}$(2)		$3.8\cdot10^{-5}$(2)		
Ho[b]	DMSO	$2.4\cdot10^{-5}$(1)		$2.3\cdot10^{-5}$(2)		

a. Quantum yield were measured by using $[Yb(Trop)_4]^-$ as standard.
b. Quantum yield were measured by using $[Er(Trop)_4]^-$as standard

The Yb complex has the highest quantum yield (1.9 %) among all the five complexes. This value is comparable with the highest quantum yield for Yb complex reported in the literature, which have quantum yield of 3.2 % and 2.4 % for Yb complex with monoporphyrinate in CH_2Cl_2.[42] The others have relatively lower quantum yields, especially Ho and Tm, but they are still measurable by using a Xenon lamp as a source of excitation.

2.4.2.3 Lifetime of excited states of Ln

The lifetimes of Yb^{3+} in $[Yb(Trop)_4]^-$ in DMSO, methanol, and water, and the lifetime of Nd in $[Nd(Trop)_4]^-$ in DMSO were measured (Table 14). They follow the same trends as their corresponding quantum yields.

The hydration state of lanthanide ion can be estimated by using an empirical formula (1), where q is the number of the water molecules bound to lanthanide ion, k_{H2O} and k_{D2O} are the rate constants of excited states of lanthanide ion in H_2O and D_2O respectively. A is a proportionality

constant related to the sensitivity of the lanthanide ion to vibronic quenching by OH oscillators, *B* is correction factor for outer sphere water molecules.

$$q = A\,(k_{H2O}\text{-}k_{D2O})\,\text{-}B \quad (1)$$

This experimental formula was first developed by Horrocks *et al.* for Eu and Tb complexes.[83, 84] Parker *et al.* extended this formula, and generated parameters applicable for Yb complexes.[32] Recently, Faulkner *et al.* modified it for the determination of *q* for Yb and Nd complexes in H_2O and MeOH solution.[44, 85]

For Yb:

$$q = k_{H2O}\text{-}k_{D2O} - 0.1,\ q = 2(k_{CH3OH}\text{-}k_{CD3OD}) - 0.1 \quad (2)$$

For Nd:

$$q = 130(k_{H2O}\text{-}k_{D2O}) - 0.4,\ q = 290(k_{CH3OH}\text{-}k_{CD3OD}) - 0.4 \quad (3)$$

(All the rate constants use μs as unit.)

Applying these formulas for Yb complex, *q* values were calculated as 1.13 in water and 0.98 in methanol. These consistently indicate that for lanthanide tropolone complexes in solution, there is one water molecule bound to the lanthanide ion. So the structure in solution is different from the structure observed in the solid state, since no coordinated solvent molecules have been observed in the structure in the solid state. This also explains the significant difference of the quantum yields in deuterated and non-deuterated solvents. The tropolone ligands in the ML_4 do not efficiently protect the Ln^{3+} cation from the non-radiative deactivations, allowing access of one molecule of solvent to the metal ion.

2.4.3 Visible luminescence

Fluorescence and phosphorescence

The Gd^{3+} ion has no energy levels below 32,000 cm^{-1}, and therefore usually cannot accept any energy from the ligand excited states. So it is regarded as a "silent" cation and used to study the ligand's electronic state when coordinated with lanthanide cations. The fluorescence and phosphorescence spectra of Gd complex are depicted in Figure 33. The excitation and absorption spectra are similar (not shown). The shift between the fluorescence band (431 nm, 23,202 cm^{-1}) and phosphorescence band (587 nm, 17,038 cm^{-1}) is 156 nm (6164 cm^{-1}). Due to the low temperature, there are some structure bands in the phosphorescence spectrum. The triplet state we measured here is consistent with the value previously reported by Croteau 595 nm (16807 cm^{-1}).[51]

The quantum yields of the ligand fluorescence were also measured by using quinine sulfate as standard (Table 13). The non-luminescent Y, La complexes have comparable quantum yields with the "free" ligand (KTrop). Their quantum yields are higher than those observed for the ligand in the luminescent complexes. This is due to the heavy atom (paramagnetic) effects.[86, 87] An external heavy atom effect can be induced by a heavy (paramagnetic) metal ion in close proximity of a chromophore, and increases the intersystem crossing yield of the chromophore, which results in a reduction of the fluorescence intensity and a concomitant increase in the phosphorescence intensity. This effect has been attributed to an enhanced spin-orbit coupling of the system which relaxes the selection rules for electronic transitions, but also to an exchange interaction of metal-unpaired electrons with the σ-electrons of the organic chromophore. The small differences in the fluorescence quantum yields with varying lanthanide ion can be explained by variation in atomic weight and magnetic moment of the ions.[88]

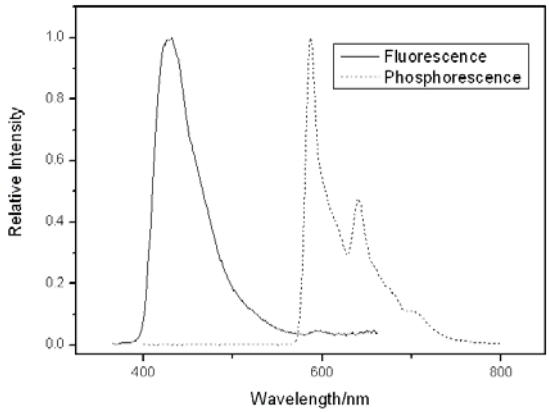

Figure 33. Fluorescence (in DMSO) and phosphorescence spectra of $[Gd(Trop)_4]^-$. The phosphorescence was measured at 77 K in DMSO with a 0.1ms decay time after excitation to discriminate phosphorescence from fluorescence.

Table 13. Quantum yield of ligands' singlet states.

	K	La	Lu	Y	Gd	Yb	Nd	Er	Ho	Tm
QY_{abs}[1]	0.0221	0.0176	0.0073	0.0127	0.0080	0.0021	0.0022	0.0020	0.0025	0.0023
QY_{rel}[2]	1.25	1.00	0.41	0.72	0.45	0.12	0.13	0.11	0.14	0.13

1. QY_{abs}: absolute quantum yield measured by using quinine sulfate in 0.5 M H_2SO_4 as standard ($\Phi = 0.54$), error 10%
2. QY_{rel}: relative quantum yield calculated using $[La(Trop)_4]$ as standard.

2.4.4 Solid state luminescence study for Yb complex.

The luminescence spectrum of Yb complexes in solid state was measured at low temperature (77 K) (Figure 34). The goal of this experiment was to measure the crystal field splitting effect under this type of symmetry (D_{2d}) of ligand field. This study is under way.

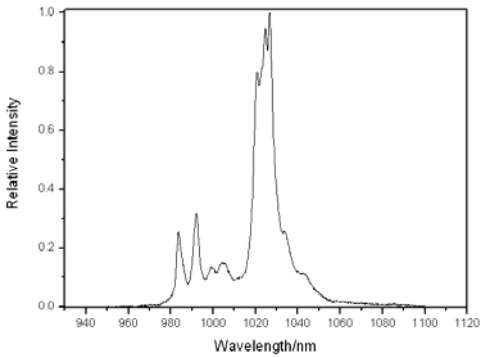

Figure 34. High resolution spectra of Yb complex in solid state (powder sample) at 77 K.

2.5 CONCLUTION

The coordination chemistry of tropolone with several lanthanide cations was studied. ML_4 complexes were synthesized, and seven single crystals were prepared and the structures are presented for the first time. Complexes were characterized by elemental analysis, IR, NMR, MS. Spectrophotometric titration indicate the presence of ML_1, ML_2, ML_3, and ML_4 complexes in solution. Preliminary photophysical studies have been carried out. The studies show that tropolone can sensitize the NIR luminescence of five lanthanide ions, due to good energy transfer between the ligand and metal ions. The structure of the $[Ln(Trop)_4]^-$ in the solid state does not match the structure in solution. In solution, there still has one water molecule bound to lanthanide that affect the quantum yields of the complexes. Luminescence of Ho^{3+} complex in solution was observed and described for the first time.

Future work:

1 Increase the stability of the complexes by connecting four tropolone chelating groups to a common backbone in order to form an octadentate ligand. This will be discussed in Chapter 3.

2 More detailed photophysical study on the mechanism of the energy transfer in the lanthanide complexes.

3.0 SYNTHESIS AND LUMINESCENT PROPERTIES OF LANTHANIDE COMPLEXES WITH AN OCTADENTATE LIGAND WHICH INCORPORATES FOUR TROPOLONE CHELATING UNITS

3.1 INTRODUCTION

In chapter 2, it has been demonstrated that tropolone is a good chelator and antenna for NIR luminescent lanthanide ions. But tropolone complexes can not be used at low concentration in solution, limiting their use for biological applications. To increase the stability of these complexes, ligands with high denticity are often used because of its entropy effect. For example, DTPA derivatives[89], *m*-terphenyl-based ligands[90], calix[4]arene derivatives[91] have been used as multidentate ligands in the NIR luminescent lanthanide complexes.

On the other hand, for NIR luminescent lanthanide complex, the protection of the lanthanide cation is very important. Due to the smaller energy gap between the excited and ground state, NIR emitting lanthanides are more sensitive to non-radiative quenching by coordinated solvent molecules. It has been shown that in the tropolone complexes, the ligands have limited ability to protect the lanthanide cations. In solution, one water molecule is bound the lanthanide cation. So the protection needs to be improved.

So we designed an octadentate ligand L_1, which incorporates four tropolone units connected through a backbone (Figure 35). This octadentate ligand could satisfy the requirement of high coordination number (8) of lanthanide and keep the tropolone chromophore as the

sensitizer to the lanthanide cations. Adding a methylene group on the seven-membered ring is expected not to change significantly the electronic structure of tropolone, and accordingly, to retain its good sensitizing ability. More importantly, by connecting the four tropolone units to a common backbone, the entropy effect will largely increase the thermodynamic stability of the complex. The protection of lanthanide cations is expected to be improved by using the proposec backbone by preventing the physical access of water molecules to the lanthanide ion.

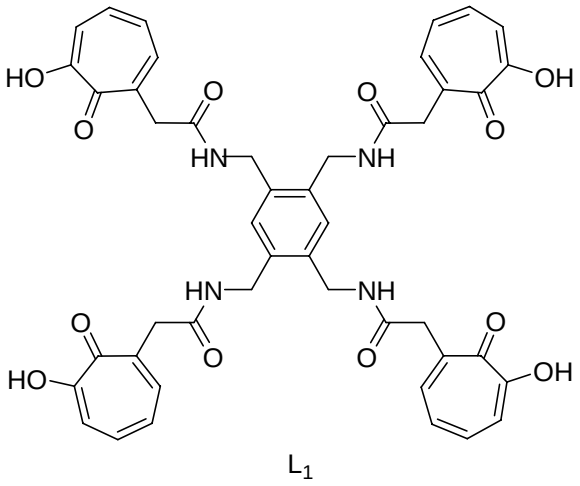

L_1

Figure 35. Structure of designed octadentate ligand L_1.

In this chapter, the synthesis and characterization of the ligand (Figure 34) and its lanthanide complexes are described. Photophysical properties of the complexes are also studied.

3.2 CACHE MODELING OF LANTHANIDE COMPLEX WITH L_1: {$[LN(L_1)]^-$}

Modeling of the lanthanide complex formed with L_1 was performed with the software CAChe[92]. The structure of the $[ML_1]^-$ was refined by performing an optimized geometry calculation in molecular mechanics using augmented MM3 parameters. The resulted structure is shown in Figure 37. The ligand acts as an octadentate ligand, coordinating lanthanide cation by its eight

oxygen atoms of the four tropolone units. The picture indicates that the access to the Ln^{3+} cation by the solvent molecules prevented by the ligand design.

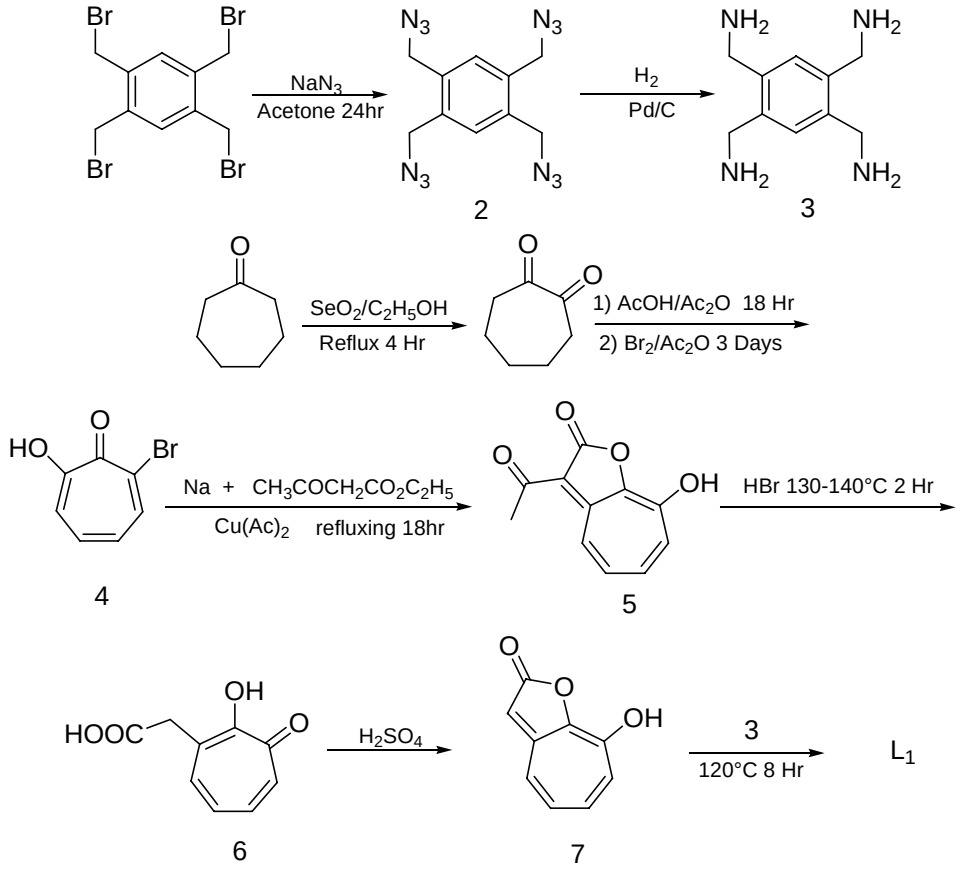

Figure 36. Synthetic route for ligand L_1.

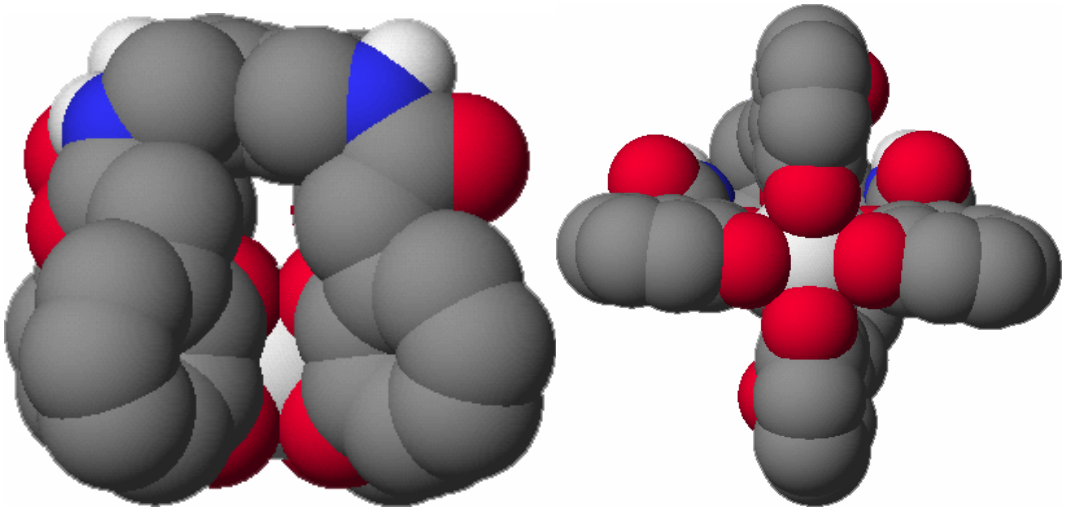

Figure 37. Different views of optimized structure (CAChe, MM3 molecular mechanics)[92] of $\{[Ln(L_1)]^-\}$.

3.3 PHOTOPHYSICAL PROPERTIES

3.3.1 Absorption, excitation and emission spectra of $[Yb(L_1)]^-$

As expected, the absorption spectrum for $[Yb(L_1)]^-$ in DMSO has similarities to the absorption spectra to the $[Ln(Trop)_4]^-$ (Figure 38). In both cases, the maxima of the absorption bands are located around 337 nm and 385 nm. This is due to the $^1\pi$-π^* transition of the four tropolone units in the octadentate ligand.

The excitation spectrum (Figure 39) of $[Yb(L_1)]^-$ was measured monitoring the emission centered on Yb^{3+} at 979 nm. This spectrum has similarities with the absorption spectrum of the complex (Figure 38), which indicates that the ligand sensitizes the luminescence of Yb through the tropolone units. Upon excitation of the ligand at 340 nm, the characteristic sharp emission of Yb at 980 nm was obtained (Figure 39). The crystal field splitting was observed (three main bands at 979, 992 and 1023 nm). This splitting is very similar to that observed for $K[Yb(Trop)_4]$ in DMSO.

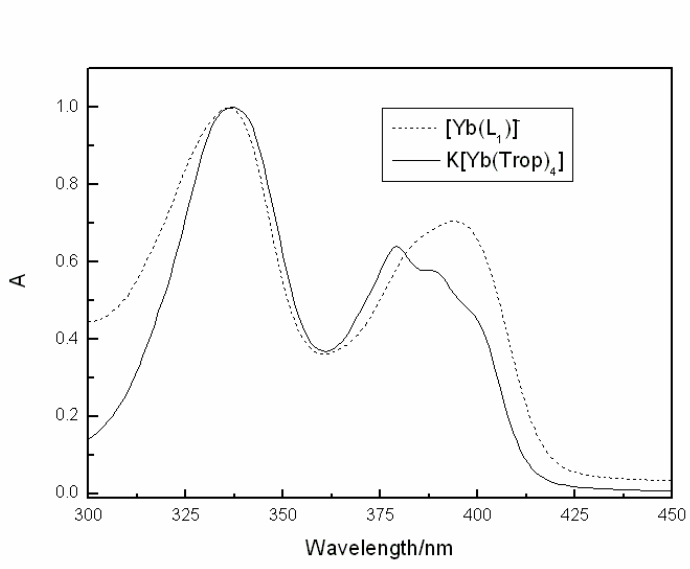

Figure 38. Normalized absorption spectra of $[Yb(L_1)]^-$ and $K[Yb(Trop)_4]$ in DMSO.

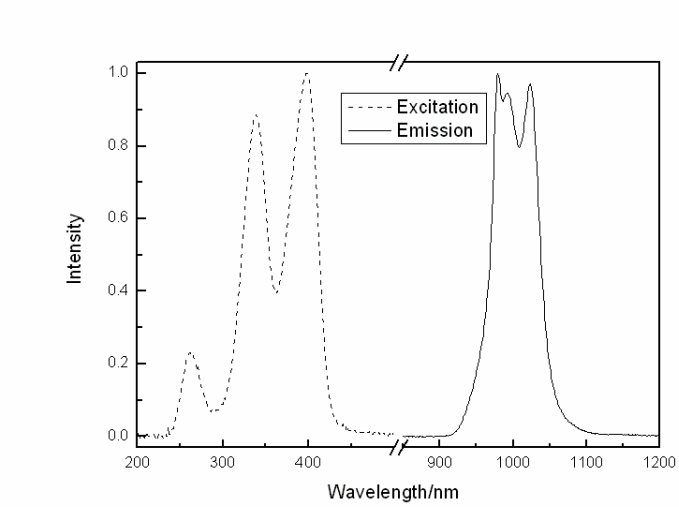

Figure 39. Normalized emission and excitation spectra of $[Yb(L_1)]^-$.

3.3.2 Overall quantum yield of the complex and lifetime of excited state of Yb^{3+} in $[Yb(L_1)]^-$

Quantum yields of sensitized emission of Yb complex in various solvents were determined by using $K[Yb(Trop)_4]$ as standard. The lifetimes were also measured. All the results are tabulated in Table 14.

Table 14. Quantum yields and lifetimes of Yb complex with L_1 in various solvent.

Solvent	deuterated		non-deuterated		$k_{q,\,solv}$ (s^{-1})[c]
	QY[a]	Lifetime (μs)[b]	QY[a]	Lifetime (μs)[b]	
DMSO	$3.6\cdot10^{-2}$	15.84(3)	$2.0\cdot10^{-2}$	12.68(4)	$1.57\cdot10^{4}$
Methanol[d]	$4.1\cdot10^{-2}$	15.5(2)	$6.1\cdot10^{-3}$	5.13(8)	$1.30\cdot10^{5}$
Water[d]	$1.8\cdot10^{-2}$	13.8(2)	$2.9\cdot10^{-3}$	2.77(2)	$2.88\cdot10^{5}$

a. Quantum yields were measured using $[Yb(Trop)_4]^-$ as reference, estimated error 10%.
b. Lifetimes are the average values of three independent measurements. λ_{ex} = 337 nm.
c. $k_{q,solv}$ is the quenching rate of the solvent. $k_{q,solv} = 1/\tau_H - 1/\tau_D$.
d. Mixture of solvents was used: 3% DMSO was used due to the limited solubility of complex.

All the quantum yields in various solvents of $[Yb(L_1)]^-$ are larger than those reported for the $K[Yb(Trop)_4]$ complex. This indicates that the introduction of the backbone provides a better

protection to the lanthanide cation, assuming the energy transfer is comparable to the tropolone complex. This assumption is supported by the result of calculation of *q* values. According to the formula developed by Faulkner *et al.*[44, 85], the *q* values for $[Yb(L_1)]^-$ were calculated as 0.06 and 0.09 in methanol and water respectively. These two values indicate that there is no water molecules bound to lanthanide ion and therefore no significant non-radiative deactivation due to O-H, N-H, C-H vibration in the first coordination sphere, which is consistent with the higher quantum yield in the $[Yb(L_1)]^-$. It is of note that the quantum yield of the $[Yb(L_1)]^-$ in water is about 12 times higher than that in $K[Yb(Trop)_4]$ as a result of improved protection.

3.3.3 Visible luminescence

The fluorescence spectra of $[Yb(L_1)]^-$ at room temperature and phosphorescence spectra of $[Gd(L_1)]^-$ at 77 K were measured and are shown in Figure 40. The fluorescence and phosphorescence spectra of the complexes with L_1 are very similar to those observed for $K[Ln(Trop)_4]$. Both phosphorescence spectra have two sharp bands at 590 nm (16,950 cm^{-1}) and 640 nm (15,625 cm^{-1}). This indicates that the singlet and triplet states of the ligand were not significantly affected by the attachment of the tropolone chelating groups to a backbone. The lifetimes of triplet states in both complexes are within the same range, 5.5±0.1 ms (587 nm and 640 nm) for $K[Gd(Trop)_4]$ and 5.8±0.3 ms (589 nm and 641 nm) for $[Gd(L_1)]^-$.

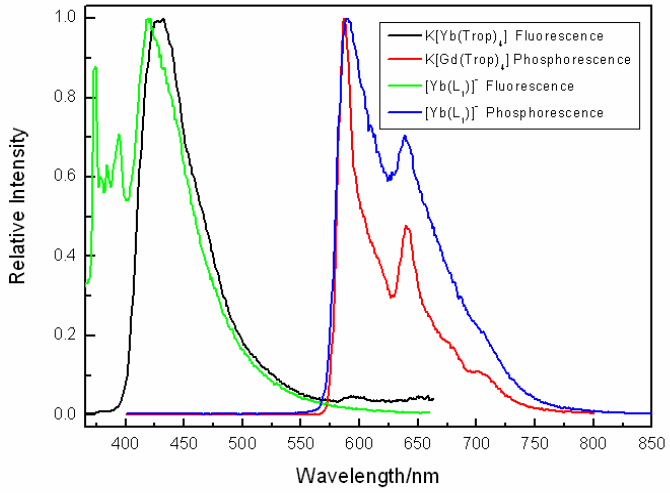

Figure 40. Normalized fluorescence spectra of $[Yb(L_1)]^-$ and $K[Yb(Trop)_4]$ and phosphorescence spectra for $[Gd(L_1)]^-$ and $K[Gd(Trop)_4]$ (λ_{ex} = 340 nm). (The phosphorescence was measured at 77 K in DMSO with a 0.1 ms delay time after excitation to distinguish phosphorescence from fluorescence).

3.3.4 Dilution experiment

The complex with the octadentate ligand is expected to have higher stability than the $K[Ln(Trop)_4]$. Due to the low solubility of $[Ln(L_1)]^-$, we evaluated the stability of the complex by using a simple dilution experiment. For a given complex, scince lanthanide cations are very labile metal ions, the more dilution, the more dissociation, which is depending on the stability constant of the complex. Therefore, the relative thermodynamic stability can be estimated by measuring the decay of the luminescence intensity upon dilution. The luminescence intensity changes upon diluting the complexes until the limit of detection of the instrument was attained were measured and are reported in Table 15 and Figure 41.

Table 15. Corrected luminescence intensities of complexes.

Dilution factor	$[Yb(Trop)_4]^-$		$[Yb(L_1)]^-$	
	Intensity[a]	Corrected intensity[b]	Intensity[a]	Corrected intensity[b]
1	1.0000	1.0000	1.0000	1.0000
2	0.8460	1.6920	0.9426	1.8852
4	0.4578	1.8312	0.6111	2.4444
8	0.1608	1.2864	0.3155	2.5240
16	0.0436	0.6976	0.1384	2.2144
32	0.0076	0.2432	0.0588	1.8816
64	0.0011	0.0704	0.0250	1.6000
128			0.0104	1.3312
256			0.0046	1.1776
512			0.0021	1.0752
1024			0.0010	1.0240
2048			0.0005	1.0240

a. The initial absorbance of both solutions was kept as A = 2.0. The initial emission intensity was normalized to 1.
b. The dilution effect was corrected by multiplying the observed intensity value by the dilution factor.

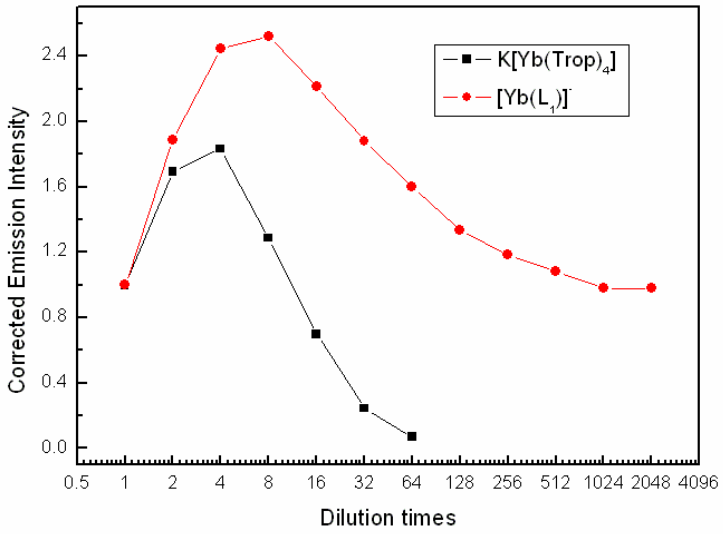

Figure 41. Corrected Yb^{3+} centered luminescence intensity vs dilution times

It can be seen from the results that for both complexes an increase in luminescence intensity can be observed at the initial 2-3 dilutions. This can be attributed to the "inner filter effect" due to the high absorbance of the initial solution (A = 2.0, in a 1 cm cell) at the excitation

wavelength (340 nm). When subsequent dilutions are carried out, the corrected luminescence intensities of both complexes decrease. This can be explained as follows: first, the solvent was not completely dry [typically, a new bottle DMSO solvent contains at least 400 ppm of water (about $5.6 \cdot 10^{-3}$ mol/L)], so the more diluted, the larger the molar ratio of water to Yb complex will be. For example, the initial molar ratio of water to Ln complex is about 168 to 1, after dilution 6, the ratio is 10,763 to 1, and 344,408 to 1 after dilution 11. Due to the larger and larger number of water molecules introduced by the dilution, ther will be a higher probability to quench Yb^{3+} emission. This quenching could happen though first or second coordination sphere mechanisms. Second, the complex might partially dissociate at low concentration. This dissociation will be more pronounced for $K[Yb(Trop)_4]$.

The observation of a signal arising from Yb^{3+} in $[Yb(L_1)]^-$ at significantly lower concentration than for [Yb(Trop)4]- is a strong indication of the higher stability of $[Yb(L_1)]^-$ in comparison to $[Yb(Trop)_4]$-. The signal of $[Yb(Trop)_4]^-$ vanished completely after the 32nd dilution factor. The signal of $[Ln(L_1)]^-$ can be observed at dilution factor of 2048 and tends to plateau. At 10^{-8} M, the Yb luminescence is still observable using a Xenon lamp as a source of excitation and further experiments will allow to determine the absolute lower limit of detection.

3.4 CONCLUSION

This chapter described synthesis of a new octadentate ligand L_1 and properties of the Gd and Yb complexes formed with this ligand. Dilution experiments indicate that, by using a common backbone to connect the four tropolone chelating units, the stability of the complex was increased significantly and the luminescence of the $[Yb(L_1)]^-$ can be observed at very low

concentration (10^{-8} mol/L). This is important for biological applications since concentration of luminescent reporters are typically in a range between 10^{-8} to 10^{-10} M.

Similar photophysical properties of the ligand tropolone and L_1 were observed, which indicates that the attachment to a backbone does not significantly affect the electronic structure of the free ligand. The ligand offers a better protection to the lanthanide ion in solution compared to the bidentate tropolone ligand. Calculations from the measured radiative rates indicate that there are no water molecules bound to lanthanide cation, and the non-radiative deactivation from high energy O-H vibration was minimized. The limitations of $K[Ln(Trop)_4]$ for imaging applications in solution, such as limited stability and incomplete protection of the metal ion, have been removed by coordinating lanthanide cations to this novel octadentate ligand The presence of the backbone does not seem to affect significantly the photophysical properties of the resulting $[Yb(L_1)]^-$ complex.

3.5 EXPERIMENTAL

3.5.1 Chemicals

All chemicals were used as received. $LnCl_3 \cdot nH_2O$ (Ln = Gd and Yb, n = 6 or 7, 99.99 %), 1,2,4,5-tetrakisbromomethylbenzene, NaN_3, 5% Pd on carbon and bromine were purchased from Aldrich. Cyclohepanone and selenium dioxide were bought from Alfa Aesar. All solvents were used as received, unless otherwise stated. All deuterated NMR solvents were purchased from Cambridge Isotope Labs and used as received.

3.5.2 Synthesis of ligand L_1

1,2,4,5-Tetrakis(azidomethyl)-benzene (2)

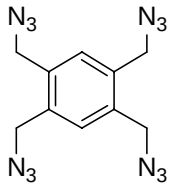

[Caution: This step is dangerous; the pure compound is explosive and should not be heated. A blast shield should also be used.]

1,2,4,5-Tetrakisbromomethyl-benzene (5.18 g, 11.5 mmol) was dissolved in acetone (300 mL). Sodium azide (10.77 g, 165.7 mmol) was added and the mixture was refluxed for 24 hours under nitrogen atmosphere whilst stirring. The reaction mixture was allowed to cool to room temperature and diluted with ether (100 mL) and water (100 mL). The organic layer was separated and washed with 200 mL of saturated sodium chloride, dried over Na_2SO_4, and the solvent removed *in vacuo* (without heating) to give the title compound as a colorless solid (3.26g, 95%). This material was used without further purification and characterization.

1,2,4,5-Tetrakis(aminomethyl)-benzene (3)

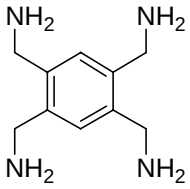

1,2,4,5-Tetrakis(azido-methyl)-benzene (**2**) (2.00 g, 6.71 mmol) was dissolved in CH_3OH (150 mL) and Pd/C (0.5 g) was added. The reaction was carried out under hydrogen overnight. The solution was filtered and evaporated under vacuum to give the title compound (1.23 g, 95%). ^{1}H NMR (DMSO-d_6, 300MHz): δ 2.70 (s, 8H, -NH_2), 3.73 (s, 8H, -CH_2NH$_2$), 7.26 (s, 2H, Ar-*H*).

2-Bromo-7-hydroxy-2,4,6-cycloheptatrien-1-one (7-bromotropolone) (4)[93]

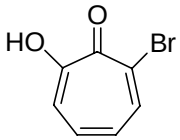

To a solution of cycloheptanone (6.80 g, 60.7 mmol) dissolved in ethanol (14 mL), selenium dioxide (6.66 g, 60.0 mmol) was added. After refluxing for 4 hours, insoluble materials were removed by filtration. The resulting mixture was distilled under reduced pressure (110 ˚C /15 mmHg) for purification to give 5.112 g of 1, 2-cycloheptadione as a yellow oily substance. To this 1, 2-cycloheptadione (5.15 g, 40.8 mmol), acetic acid (2 mL) and acetate anhydride (0.2 mL) were added. After stirring at room temperature for 18 hr and then cooling to 0 ˚C, a solution of bromine (4.1 mL) and acetic acid (4 mL) was gradually added drop wise thereto. This mixture was allowed to react at room temperature for 3 days. The resulting precipitate was recovered by filtration. A suspension of this precipitate in water was adjusted to pH 3-4 with 20% sodium hydroxide. The precipitate was recovered by filtration to give a crude crystal of 7-bromotropolone. Recrystallized from cyclohexane gave the title compound as as yellow needles (0.976 g, 8 %). Mp: 104-105 ˚C. EI-MS: *m/z* $[M]^+$ 199.947647 (Calc. 199.947291 for $C_7H_5O_2Br$). ^1H NMR ($(CD_3)_2CO$, 300MHz): δ 7.00 (t, J = 10 Hz, 1H), 7.38 (d, J = 10.5 Hz, 1H), 7.55 (t, J = 10 Hz, 1H), 8.32 (d, J = 9.6 Hz, 1H). IR (KBr, cm^{-1}): 3568 (O-H), 3215 (C-H), 1603, 1591 (C=O), 1544, 1477, 1458, 1413, 1361, 1306, 1242, 1204, 1076, 994, 957, 897, 778, 749.

3-Acetyl-8-hydroxy-1-oxaazulan-2-one (5)[94]

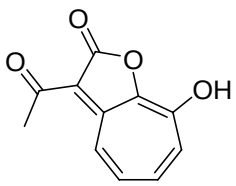

To a solution of ethyl sodioacetoacetate prepared by dissolving sodium (12.0 g, 0.522 mol) in a mixture of ethyl acetoacetate (90 g, 0.9 mol) and dry dioxane (160 mL), 2-Bromo-7-hydroxy-2,4,6-cyclo-heptatrien-1-one (4) (20.0 g, 0.100 mol) and copper acetate (400 mg, 2.2 mmol) were added; the mixture was then refluxed for 18 hours. After the addition of water (200 mL), the mixture was shaken with ether (200 mL) and the aqueous layer was acidified with 6 N hydrochloric acid and allowed to stand overnight. The crystals thereby formed were collected and washed with chloroform to give the product. Recrystallization from a large amount of acetone gave the title compound as yellow silky needles (19.1 g, 94 %). Mp: 285-287 ˚C (decomp.). EI-MS: *m/z* $[M]^+$ 204.041960 (Calc. 204.042259 for $C_{11}H_8O_4$). ^1H NMR ($(CD_3)_2CO$, 300MHz): δ 2.46 (s, 3H, -CH_3), 7.59-7.76 (m, 3H, Ar-*H*), 9.20 (d, *J* = 11 Hz, 1H, Ar-*H*). IR (KBr, cm^{-1}): 3424 (O-H), 3056 (C-H), 1736 (C=O), 1623 (C=O), 1587, 1506, 1465, 1392, 1357, 1311, 1285, 1242, 1190, 1147, 1091, 1024, 929, 780, 748, 702, 662, 613.

2-Hydroxy-3-oxo-1,4,6-cycloheptatriene-1-acetic acid (6)[94]

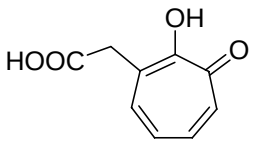

A mixture of 3-acetyl-8-hydroxy-1-oxazulan-2-one (4.0 g, 19.6 mmol) and concentrated hydrobromic acid (30 mL) was heated at 130-140 ˚C for 2 hours. The mixture was poured into ice-water (50 g) and adjusted to pH 3 with a potassium hydroxide solution; the crystals thereby obtained were collected by filtration, affording the title compound (2.7 g, 76 %). Mp: 174-177 ˚C (decomp.). EI-MS: *m/z* $[M]^+$ 180. ^1H NMR ($(CD_3)_2CO$, 300MHz): δ 3.81 (s, 2H, CH_2-COOH) 7.12 (t, *J* = 10 Hz, 1H), 7.35 (d, *J* = 10.5 Hz, 1H), 7.45 (t, *J* = 10 Hz, 1H), 7.73 (d, *J* = 9.0 Hz, 1H), 10.23 (b, 1H). IR (KBr, cm^{-1}): 3447, 3225, 2942, 1701 (C=O, acid), 1610 (C=O, ring), 1595, 1540, 1472, 1420, 1388, 1318, 1270, 1241, 1216, 1181, 947, 858, 726, 701, 650.

8-Hydroxy-2H-cyclohepta[b]furan-2-one (7)[94]

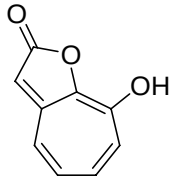

A solution of 2-Hydroxy-3-oxo-1,4,6-cycloheptatriene-1-acetic acid (0.40g, 1.96 mmol) in concentrated sulfuric acid (1 mL) was poured into ice-water to give the title compound (0.22 g, 60 %). Mp: 223-224 ˚C (decomp.). EI-MS: *m/z* $[M]^+$ 162. ^{1}H NMR ($(CD_3)_2CO$, 300MHz): δ 5.54 (s, 1H, -C*H*-CO)), 6.94-7.12 (m, 3H), 7.50 (d, J = 11.4 Hz, 1H).

N,N',N'',N'''-[1,2,4,5-Phenylenetetra(methylene)]tetrakis-(2-hydroxy-3-oxo- 1,4,6-cycloheptatriene-1-)acetamide (L_1)

8-Hydroxy-2H-cyclohepta[b]furan-2-one (**7**) (32.4 mg, 0.2 mmol) and 1,2,4,5-tetrakis(aminomethyl)-benzene (**3**) (9.7 mg, 0.05 mmol) were dissolved in dry DMF (10 mL). The reaction mixture was heated at 80ºC for 6 hours. The DMF was evaporated and the resulted solid was dispersed in methanol, filtered, and washed using methanol three times to give the title compound (25.3 mg, 60%). MS-ESI: m/z $[M+Na]^+$ 865.2. ^{1}H NMR (DMSO-d_6, 300MHz): δ 3.65 (s, 8H, -CH_2-CONH), 4.30 (d, J = 5.4 Hz, 8H, Ar-CH_2-NH), 7.01 (t, J = 10 Hz, 4H), 7.22-7.26 (m, 6H), 7.33 (t, J = 10 Hz, 4H), 7.60 (d, J = 9.3 Hz, 4H), 8.42 (t, J = 5.4 Hz, 4H, -N*H*-), 10.18 (b, 4H). IR (KBr, cm^{-1}): 3284 (NH), 3081, 2924, 1644 (C=O of amide), 1610 (C=O of ring), 1595, 1540, 1472, 1420, 1388, 1318, 1270, 1241, 1216, 1181, 947, 858, 726, 701, 650.

3.5.3 Synthesis of lanthanide complexes

Synthesis of the complexes was carried in high dilution conditions. 0.010 mmol of KOH in methanol was added to a solution of 0.0025 mmol of ligand in 150 ml methanol. The resulted

solution was refluxed and then added 0.0025 mmol $LnCl_3 \cdot nH_2O$ (Ln = Gd and Yb) in 150 ml methanol in 6 hours. The solution was kept refluxing for another 6 hours and evaporated to 20 ml. The resulted precipitate was filtered, washed three times with methanol and dried *in vacuo* over P_2O_5 for 48 hours. ESI MS for Yb complex: 1014.0[$\mathbf{L_1}$+Yb-2H], 1036.1[$\mathbf{L_1}$+Yb-3H+Na], 1052.0[$\mathbf{L_1}$+Yb-3H+K].

4.0 STUDIES OF NIR LUMINESCENT LANTHANIDE COMPLEXES FORMED WITH NITRO- AND AMINO- SUBSTITUTED TROPOLONE

4.1 INTRODUCTION

The mechanism of ligand to lanthanide energy transfer is one of the important research areas in lanthanide coordination chemistry because the information on energy transfer will help scientists to rationally design and synthesize efficiently luminescent lanthanide complexes with controlled properties.

A useful methodology in studying the energy transfer mechanism is to utilize structure related ligands to carry out comparative luminescence studies between the corresponding complexes. As an example, Verhoeven *et al.*[95] studied the photophysical properties of DTPA complexes of NIR lanthanide ions with two different sensitizers: erosin and fluorescein. Eosin is a tetrabromo-derivative of fluorescein, and it has a triplet energy level located at lower energy than fluorescein. Eosin complexes of Yb^{3+} and Nd^{3+} have higher quantum yields in comparison to the fluorescein analogue, but it is not the case for the Er^{3+} complex. Different results were obtained by van Veggel *et al.*[29] in their study of sensitizing NIR lanthanide ion by triphenyl-based ligands, which have fluorescein, eosin and erythrosin as the antenna groups. They found that the complexes with fluorescein have the highest quantum yields among the three ligands. Van Deun *et al.*[96] and Yanagina *et al.*[97] used 8-quinoline and its chloro- and bromo- derivatives as ligands to study the NIR luminescent complexes of Er^{3+} and Nd^{3+}, respectively. They both

found that the introduction of halogen atom strongly increases the quantum yields (30% and 250% respectively) because of the heavy-atom effect.[86-88]

We choose to substitute the tropolone with $-NO_2$ and $-NH_2$ groups. Nitro and amino substituting groups have very different effects on the electronic structure of organic compounds. Nitro is strongly electron-withdrawing and amino is strongly electron-donating. It will be interesting to systematically study the effect of these two groups on tropolone ligand and on the luminescence properties of their corresponding lanthanide complexes. In this chapter, we describe the synthesis of nitro and amino substituted tropolone ligands and their corresponding lanthanide complexes. The preliminary photophysical properties of the Yb^{3+}, Nd^{3+} and Gd^{3+} complexes are reported.

4.2 LIGAND AND COMPLEXES SYNTHESIS

4.2.1 Synthesis of 2-hydroxy-5-nitro-2,4,6-cycloheptatrien-1-one (HNTP).[47]

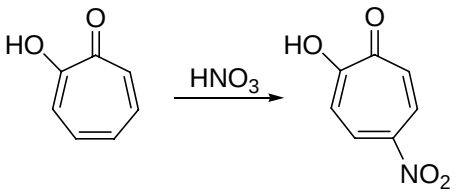

A solution of tropolone (1.00 g, 8.2 mmol) in water (40 mL) was treated with cold 1:1 nitric acid (40 ml). Crystallization occurred within 10 to 15 minutes. The product was immediately centrifugated, washed twice with cold water and dried to give the title compound (0.48 g, 35 %). Mp: 191-193 ˚C. EI-MS: *m/z* $[M]^+$ 167.021789 (Calcd. 167.021858 for $C_7H_5O_4N$). ^1H NMR ($(CD_3)_2CO$), 300 MHz): δ 7.40 (d, J = 12 Hz, 2H), 8.58 (d, J = 12 Hz, 2H). IR (KBr, cm^{-1}):

3208, 3059, 1613 (C=O), 1566, 1526, 1458, 1420, 1314, 1267, 1231, 1200, 1088, 1042, 887, 864, 828, 750, 724, 557, 490.

4.2.2 Synthesis of 2-hydroxy-5-amino-2,4,6-cycloheptatrien-1-one (HMTP)[98]

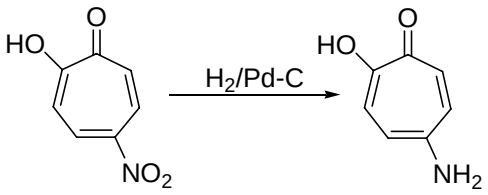

5-Nitrotropolone (2.32 g, 15.36 mmol) was suspended in ethanol (100 ml). 5% Pd/C (20 mg) was added as a catalyst and the reaction was stirred under a hydrogen atmosphere at room temperature for 24 hours. The resulted dark-green solution was filtered to reclaim the catalyst, and the solvent was removed to give the title compound as an orange powder (1.75 g, 92 %). Mp: 178-179 ˚C. EI-MS: *m/z* $[M]^+$ 137.048168 (Calcd. 137.047679 for $C_7H_7O_2N$). ^1H NMR (CD_3OD, 300MHz): δ 6.89 (d, J = 12.6 Hz, 2H), 7.28 (d, J = 12 Hz, 2H). IR (KBr, cm^{-1}): 3422, 3338, 3208, 1662 (C=O), 1529, 1513, 1443, 1423, 1318, 1249, 1212, 1141, 953, 893, 845, 776, 665, 624, 580, 495.

4.2.3 Synthesis of complexes

The complexes were synthesized as follow: 0.04 mmol of KOH in methanol was added to a solution of 0.04 mmol of HNTP or HMTP in 10 ml methanol. To the resulted solution, 0.01 mmol of $LnCl_3 \cdot nH_2O$ (Ln = Nd, Gd, Yb) in 10 ml methanol was added. The solvent was stirred for 2 hours and the resulted precipitate was filtered, washed three times with methanol and dried *in vacuo* over P_2O_5 for 48 hours. For both ligands, we synthesized their complexes with Nd^{3+}, Gd^{3+} and Yb^{3+}.

For Gd and Yb complexes with HNTP, $[LnL_4]^-$ ion peaks were found in the ESI-MS spectra at 821.8 and 838.0 respectively. This could be the indication of isolation of ML_4 type of complexes. More analysis will be performed, such as elemental analysis, in the future. The following study were based the assumption that the complexes mainly formed in solution are ML_4.

The complexes studied here were abbreviated as follow: $[Ln(NTP)_4]^-$ and $[Ln(MTP)_4]^-$ (Ln = Nd, Gd, Yb).

4.3 PHOTOPHYSICAL PROPERTIES

4.3.1 Absorption, luminescence spectra and excitation spectra of Yb^{3+} and Nd^{3+} complexes

The absorption and excitation spectra of $[Yb(NTP)_4]^-$ (Figure 42) were used as representation of the absorption spectra of $[Ln(NTP)_4]^-$. It can be observed that the intensities maxima of the absorption and excitation spectra do not match. Two absorption bands with maxima located at 340 nm and 468 nm can be observed. The maximum of the excitation band is located at 400 nm. This indicates that not all the electronic states in NTP can sensitize lanthanide luminescence. The absorption and excitation spectra of $[Yb(MTP)_4]^-$ (Figure 43) are very similar.

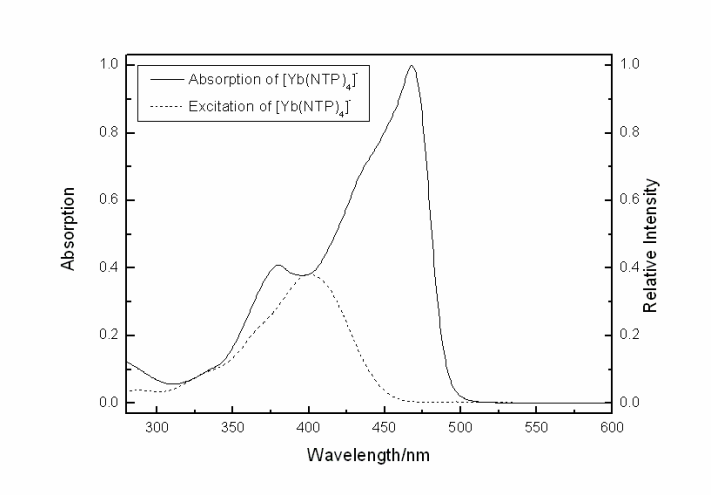

Figure 42. Absorption and excitation spectra of $[Yb(NTP)_4]^-$.

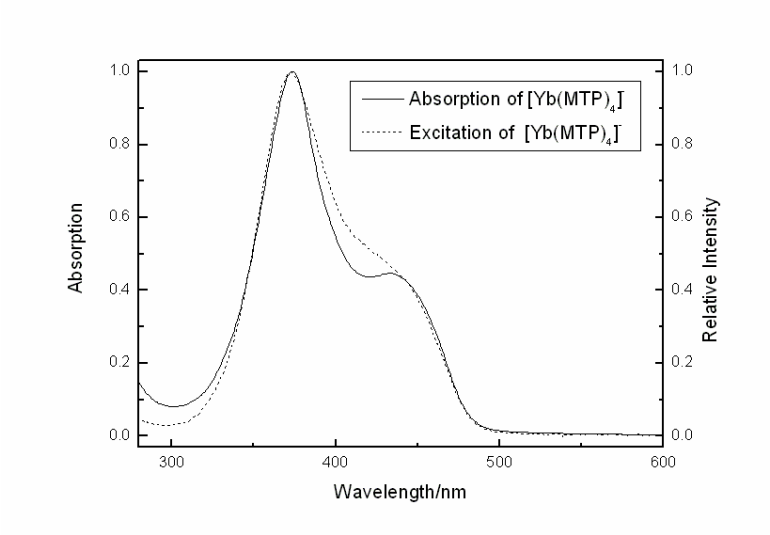

Figure 43. Absorption and excitation spectra of $[Yb(MTP)_4]^-$.

Upon excitation of NTP and MTP complexes at 400 nm and 373 nm respectively, the characteristic emission spectra of Yb and Nd were obtained (Figure 44). This indicates that both of these two ligands can sensitize the NIR luminescence of both cations. It is important to notice from the excitation spectra of $[Yb(MTP)_4]^-$ that the MTP complexes can be excited at low energy such as 450-470 nm, an advantage for imaging applications.

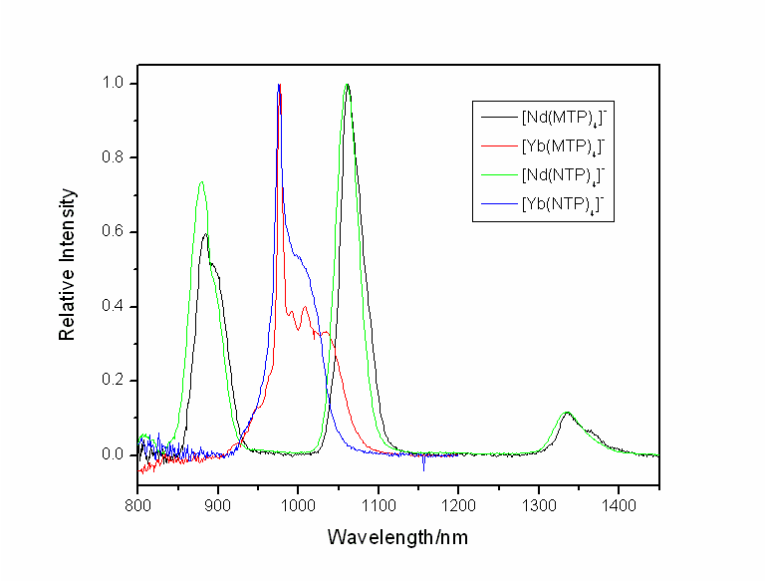

Figure 44. Normalized emission spectra of four complexes in DMSO (10^{-5} M) at room temperature, for $[Ln(NTP)_4]^-$, λ_{ex} = 400 nm; for $[Ln(MTP)_4]^-$, λ_{ex} = 373 nm.

4.3.2 Quantum yields and lifetimes of complexes

Quantum yields of the complexes in DMSO as well as the lifetimes were measured and are shown in Table 16.

Quantum yields in DMSO for all the complexes were lower compared with the corresponding $[Ln(Trop)_4]^-$. The quantum yields for MTP Yb^{3+} and Nd^{3+} complexes were higher than those for the corresponding NTP complexes with the following order of quantum yields: troplone > MTP > NTP.

The lifetimes of NTP Yb^{3+} and Nd^{3+} complexes are in the same range as those recorded for the corresponding tropolone complexes. The lifetime of $[Nd(NTP)_4]^-$ (1.4 μs) is longer than that for $[Nd(Trop)_4]^-$ (1.1 μs). Although MTP complexes have higher quantum yields than NTP complexes, shorter lifetimes have been measured in comparison to NTP complexes.

Table 16. Quantum yields and lifetimes of Nd and Yb complexes with HNTP and HMTP ligands.

	NTP		MTP	
	QY[a,b]	Lifetime(μs)[d]	QY[a,c]	Lifetime(μs)[d]
Nd	$1.0 \cdot 10^{-3}$(1)	1.41(2)	$1.4 \cdot 10^{-3}$(1)	0.73(1)
Yb	$5.6 \cdot 10^{-2}$(5)	10.09(3)	$9.9 \cdot 10^{-3}$(7)	5.74(3)

a. Quantum yields were measured in DMSO (10^{-5} M), using $K[Yb(Trop)_4]$ as reference.
b. λ_{ex} = 400 nm.
c. λ_{ex} = 373 nm.
d. Lifetimes are the average values of three independent measurements. λ_{ex} = 337 nm.

Lifetime of Yb complex in methanol

Luminescence lifetime values of 14.16 μs and 1.73 μs were obtained in d_4-MeOH and h_4-MeOH respectively for $[Yb(NTP)_4]^-$. Using the empirical formula developed by Faulkner *et al.*[44, 85], the *q* value was calculated as 0.91. For $[Yb(MTP)_4]^-$, the *q* value is 0.97 (12.35 μs and 1.62 μs in d_4-MeOH and h_4-MeOH respectively). This indicates that in both cases, one MeOH molecule is bound to the lanthanide ion in solution, which is consistent with the results obtained for the parent $[Ln(Trop)_4]^-$. The substituted tropolone complexes exhibit the same degree of protection of the Ln^{3+} cations

4.3.3 Visible luminescence

The fluorescence spectra of $[Gd(NTP)_4]^-$ and $[Gd(MTP)_4]^-$ at room temperature and phosphorescence spectra at 77 K were measured and are depicted in Figures 45 and 46 respectively. For comparison, the fluorescence and phosphorescence spectra of $K[Gd(Trop)_4]$ are also shown. The estimated singlet and triplet state energies for the three ligands are listed in Table 17. Compared to those of $K[Gd(Trop)_4]$, the singlet states of NTP and MTP are located about 3,000 cm^{-1} lower in energy. The triplet states of NTP and MTP are located about 1,500 cm^{-1} and 2,300 cm^{-1} lower in energy respectively than the triplet state of tropolone.

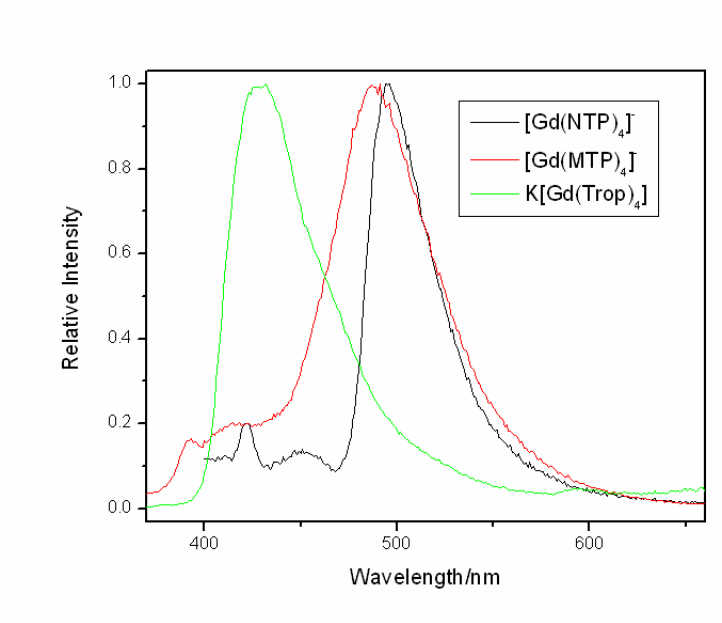

Figure 45. Fluorescence spectra of $[Gd(NTP)_4]^-$ (λ_{ex} = 400 nm), $[Gd(MTP)_4]^-$ (λ_{ex} = 373 nm), $K[Gd(Trop)_4]$ (λ_{ex} = 340 nm) in DMSO.

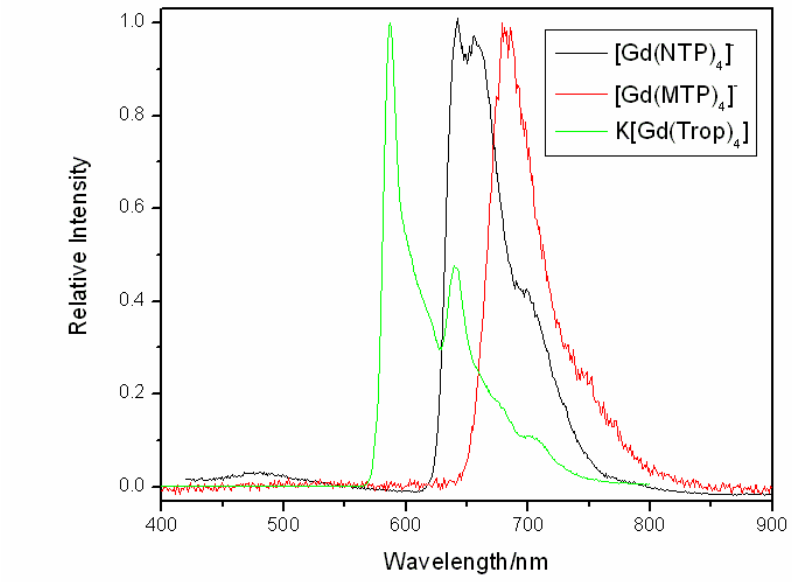

Figure 46. Phosphorescence spectra of $[Gd(NTP)_4]^-$ (λ_{ex} = 400 nm), $[Gd(MTP)_4]^-$ (λ_{ex} = 373 nm), $K[Gd(Trop)_4]$ (λ_{ex} = 340 nm) in DMSO at 77 K with 0.1 ms delay time.

Table 17. Singlet and triplet states of NTP and MTP and Trop in lanthanide complexes.

	Singlet (cm^{-1})	Triplet (cm^{-1})
$K[Gd(Trop)_4]$	23,202	17,038
$[Gd(NTP)_4]^-$	20,202	15,576
$[Gd(MTP)_4]^-$	20,450	14,706

4.4 CONCLUTIONS

From the experimental data, we obtained the following conclusions:

The presence of the substituting groups $-NO_2$ and $-NH_2$ affect the singlet and triplet electronic states of tropolone in shofting these at lower energy.

The attachment of $-NO_2$ and $-NH_2$ to the tropolone results in the red-shift of the absorption and the excitation spectra. This is very useful for imaging applications since the lanthanide complexes can be excited at lower energy (470 nm).

Although the triplet states have been significantly lowered, the quantum yields of the Nd^{3+} and Yb^{3+} complexes of NTP and MTP are smaller than those of the corresponding tropolone complexes, and are within the same range. This indicates that there are some other factors controlling the overall quantum yields, and the mechanism of ligand to lanthanide energy transfer needs more investigation.

4.5 FUTURE WORK

The complexes need to be fully characterized: identifying species in solution, and evaluating stability constants.The detailed photophysical properties of the complexes will be investigated. The mechanism of energy transfer will be rationalized.

5.0 REFERENCE

1. Weissleder, R.; Ntziachristos, V., *Nature medicine* **2003,** 9, 123-8.
2. Frangioni, J. V., *Current Opinion in Chemical Biology* **2003,** 7, 626-634.
3. Stolik, S.; Delgado, J. A.; Perez, A.; Anasagasti, L., *Journal of Photochemistry and Photobiology, B: Biology* **2000,** 57, 90-93.
4. Lin, Y.; Weissleder, R.; Tung, C.-H., *Bioconjugate Chemistry* **2002,** 13, 605-610.
5. Flanagan, J. H., Jr.; Khan, S. H.; Menchen, S.; Soper, S. A.; Hammer, R. P., *Bioconjugate Chemistry* **1997,** 8, 751-756.
6. Zaheer, A.; Wheat, T. E.; Frangioni, J. V., *Molecular Imaging* **2002,** 1, 354-364.
7. Nakayama, A.; Bianco Antonio, C.; Zhang, C.-Y.; Lowell Bradford, B.; Frangioni John, V., *Molecular imaging* **2003,** 2, 37-49.
8. Green, M., *Angewandte Chemie, International Edition* **2004,** 43, 4129-4131.
9. Derfus, A. M.; Chan, W. C. W.; Bhatia, S. N., *Nano Letters* **2004,** 4, 11-18.
10. Buenzli, J. C. G.; Choppin, G. R.; Editors, *Lanthanide Probes in Life, Chemical and Earth Sciences: Theory and Practice*. 1989; p 432 pp.
11. Weissman, S. I., *Journal of Chemical Physics* **1942,** 10, 214-17.
12. Beeby, A.; Botchway, S. W.; Clarkson, I. M.; Faulkner, S.; Parker, A. W.; Parker, D.; Williams, J. A. G., *Journal of Photochemistry and Photobiology, B: Biology* **2000,** 57, 83-89.
13. Faulkner, S.; Matthews, J. L., *Comprehensive Coordination Chemistry II* **2004,** 9, 913-944.
14. Mathis, G., *Journal of Biomolecular Screening* **1999,** 4, 309-313.
15. Hemmila, I.; Mukkala, V. M., *Critical Reviews in Clinical Laboratory Sciences* **2001,** 38, 441-519.
16. Wong, K.-L.; Kwok, W.-M.; Wong, W.-T.; Phillips, D. L.; Cheah, K.-W., *Angewandte Chemie, International Edition* **2004,** 43, 4659-4662.
17. Piszczek, G.; Maliwal, B. P.; Gryczynski, I.; Dattelbaum, J.; Lakowicz, J. R., *Journal of Fluorescence* **2001,** 11, 101-107.
18. Piszczek, G.; Gryczynski, I.; Maliwal, B. P.; Lakowicz, J. R., *Journal of Fluorescence* **2002,** 12, 15-17.
19. Sabbatini, N.; Guardigli, M.; Lehn, J. M., *Coordination Chemistry Reviews* **1993,** 123, 201-28.
20. Hebbink, G. A.; Klink, S. I.; Grave, L.; Oude Alink, P. G. B.; Van Veggel, F. C. J. M., *ChemPhysChem* **2002,** 3, 1014-1018.
21. Yang, C.; Fu, L.-M.; Wang, Y.; Zhang, J.-P.; Wong, W.-T.; Ai, X.-C.; Qiao, Y.-F.; Zou, B.-S.; Gui, L.-L., *Angewandte Chemie, International Edition* **2004,** 43, 5010-5013.
22. Hayes, A. V.; Drickamer, H. G., *Journal of Chemical Physics* **1982,** 76, 114-25.
23. Sato, S.; Wada, M., *Bulletin of the Chemical Society of Japan* **1970,** 43, 1955-62.

24. Forster, T., *Discussions of the Faraday Society* **1959,** No. 27, 7-17.
25. Forster, T., *Ann. Physik [6 Folge]* **1948,** 2, 55-75.
26. Dexter, D. L., *Journal of Chemical Physics* **1953,** 21, 836-50.
27. Faulkner, S.; Beeby, A.; Carrie, M. C.; Dadabhoy, A.; Kenwright, A. M.; Sammes, P. G., *Inorganic Chemistry Communications* **2001,** 4, 187-190.
28. Horrocks, W. D., Jr.; Bolender, J. P.; Smith, W. D.; Supkowski, R. M., *Journal of the American Chemical Society* **1997,** 119, 5972-5973.
29. Hebbink, G. A.; Grave, L.; Woldering, L. A.; Reinhoudt, D. N.; van Veggel, F. C. J. M., *Journal of Physical Chemistry A* **2003,** 107, 2483-2491.
30. Stein, G.; Wurzberg, E., *Journal of Chemical Physics* **1975,** 62, 208-13.
31. Siebrand, W., *Journal of Chemical Physics* **1967,** 46, 440-7.
32. Beeby, A.; Clarkson, I. M.; Dickins, R. S.; Faulkner, S.; Parker, D.; Royle, L.; de Sousa, A. S.; Williams, J. A. G.; Woods, M., *Journal of the Chemical Society, Perkin Transactions 2: Physical Organic Chemistry* **1999**, 493-504.
33. Werts, M. H. V.; Woudenberg, R. H.; Emmerink, P. G.; van Gassel, R.; Hofstraat, J. W.; Verhoeven, J. W., *Angewandte Chemie, International Edition* **2000,** 39, 4542-4544.
34. Klink, S. I.; Keizer, H.; Van Veggel, F. C. J. M., *Angewandte Chemie, International Edition* **2000,** 39, 4319-4321.
35. Klink, S. I.; Alink, P. O.; Grave, L.; Peters, F. G. A.; Hofstraat, J. W.; Geurts, F.; van Veggel, F. C. J. M., *Journal of the Chemical Society, Perkin Transactions 2* **2001**, 363-372.
36. Pope, S. J. A.; Kenwright, A. M.; Heath, S. L.; Faulkner, S., *Chemical Communications (Cambridge, United Kingdom)* **2003**, 1550-1551.
37. Faulkner, S.; Carrie, M.-C.; Pope, S. J. A.; Squire, J.; Beeby, A.; Sammes, P. G., *Dalton Transactions* **2004**, 1405-1409.
38. Pope, S. J. A.; Coe, B. J.; Faulkner, S.; Bichenkova, E. V.; Yu, X.; Douglas, K. T., *Journal of the American Chemical Society* **2004,** 126, 9490-9491.
39. Hasegawa, Y.; Ohkubo, T.; Sogabe, K.; Kawamura, Y.; Wada, Y.; Nakashima, N.; Yanagida, S., *Angewandte Chemie, International Edition* **2000,** 39, 357-360.
40. Goncalves e Silva, F. R.; Malta, O. L.; Reinhard, C.; Guedel, H.-U.; Piguet, C.; Moser, J. E.; Buenzli, J.-C. G., *Journal of Physical Chemistry A* **2002,** 106, 1670-1677.
41. He, H.; Guo, J.; Zhao, Z.; Wong, W.-K.; Wong, W.-Y.; Lo, W.-K.; Li, K.-F.; Luo, L.; Cheah, K.-W., *European Journal of Inorganic Chemistry* **2004**, 837-845.
42. Foley, T. J.; Harrison, B. S.; Knefely, A. S.; Abboud, K. A.; Reynolds, J. R.; Schanze, K. S.; Boncella, J. M., *Inorganic Chemistry* **2003,** 42, 5023-5032.
43. Shavaleev, N. M.; Moorcraft, L. P.; Pope, S. J. A.; Bell, Z. R.; Faulkner, S.; Ward, M. D., *Chemical Communications (Cambridge, United Kingdom)* **2003**, 1134-1135.
44. Davies, G. M.; Aarons, R. J.; Motson, G. R.; Jeffery, J. C.; Adams, H.; Faulkner, S.; Ward, M. D., *Dalton Transactions* **2004**, 1136-1144.
45. Parker, D.; Williams, J. A. G., *Journal of the Chemical Society, Dalton Transactions: Inorganic Chemistry* **1996**, 3613-3628.
46. Miller, T. A.; Jeffery, J. C.; Ward, M. D.; Adams, H.; Pope, S. J. A.; Faulkner, S., *Dalton Transactions* **2004**, 1524-1526.
47. Doering, W. v. E.; Knox, L. H., *Journal of the American Chemical Society* **1951,** 73, 828-38.
48. Muetterties, E. L.; Wright, C. M., *Journal of the American Chemical Society* **1965,** 87, 4706-17.

49. Shoute, L. C. T.; MacKenzie, V. J.; Falk, K. J.; Sinha, H. K.; Warsylewicz, A.; Steer, R. P., *Physical Chemistry Chemical Physics* **2000,** 2, 1-9.
50. Breheret, E. F.; Martin, M. M., *Journal of Luminescence* **1978,** 17, 49-60.
51. Croteau, R.; Leblanc, R. M., *Photochemistry and Photobiology* **1978,** 28, 33-8.
52. Melhuish, W. H., *Journal of Physical Chemistry* **1961,** 65, 229-35.
53. Petoud, S.; Cohen, S. M.; Buenzli, J.-C. G.; Raymond, K. N., *Journal of the American Chemical Society* **2003,** 125, 13324-13325.
54. Sheldrick, G. M., *SHELXS-97, Program for crystal structure refinement, University of G?ttingen, Germany* **1997**.
55. Sheldrick, G. M., *SHELXS-97, Program for crystal structure determination, University of G?ttingen, Germany* **1997**.
56. Sheldrick, G. M., *SADABS, Program for Siemens area detector absorption correction, University of Gottingen, Germany* **1996**.
57. Farrugia, L. J., *Journal of Applied Crystallography* **1997,** 30, 565.
58. Bruno, I. J.; Cole, J. C.; Edgington, P. R.; Kessler, M.; Macrae, C. F.; McCabe, P.; Pearson, J.; Taylor, R., *Acta Crystallographica, Section B: Structural Science* **2002,** B58, 389-397.
59. McArdle, P., *Journal of Applied Crystallography* **1995,** 28, 65.
60. Grzymalski, Z.; Jezowska-Trzebiatowska, B.; Ziolkowski, J., *Bulletin de l'Academie Polonaise des Sciences, Serie des Sciences Chimiques* **1965,** 13, 475-80.
61. Selbin, J.; Ortego, J. D., *Journal of Inorganic and Nuclear Chemistry* **1968,** 30, 313-17.
62. Bagnall, K. W.; Bhandari, A. M.; Brown, D.; Lidster, P. E.; Whittaker, B., *Journal of the Chemical Society, Dalton Transactions: Inorganic Chemistry (1972-1999)* **1975**, 1249-52.
63. Desiraju, G. R., *Accounts of Chemical Research* **1996,** 29, 441-449.
64. Jeffrey, G. A.; Maluszynska, H.; Mitra, J., *International Journal of Biological Macromolecules* **1985,** 7, 336-48.
65. Kepert, D. L., *Progress in Inorganic Chemistry* **1978,** 24, 179-249.
66. Davis, A. R.; Einstein, F. W. B., *Acta Crystallographica, Section B: Structural Crystallography and Crystal Chemistry* **1978,** B34, 2110-15.
67. Davis, A. R.; Einstein, F. W. B., *Inorganic Chemistry* **1975,** 14, 3030-5.
68. Tranqui, D.; Tissier, A.; Laugier, J.; Boyer, P., *Acta Crystallographica, Section B: Structural Crystallography and Crystal Chemistry* **1977,** B33, 392-7.
69. Kira, M.; Zhang, L. C.; Kabuto, C.; Sakurai, H., *Organometallics* **1998,** 17, 887-892.
70. Anderson, T. J.; Neuman, M. A.; Melson, G. A., *Inorganic Chemistry* **1974,** 13, 1884-90.
71. Davis, A. R.; Einstein, F. W. B., *Inorganic Chemistry* **1974,** 13, 1880-4.
72. Tedeschi, C.; Azema, J.; Gornitzka, H.; Tisnes, P.; Picard, C., *Dalton Transactions* **2003**, 1738-1745.
73. Shannon, R. D., *Acta Crystallographica, Section A: Crystal Physics, Diffraction, Theoretical and General Crystallography* **1976,** A32, 751-67.
74. Gampp, H.; Maeder, M.; Meyer, C. J.; Zuberbuehler, A. D., *Talanta* **1985,** 32, 1133-9.
75. Poh, B.-L.; Siow, H.-L., *Australian Journal of Chemistry* **1980,** 33, 491-7.
76. Reisfeld, R.; Eyal, M.; Greenberg, E.; Joergensen, C. K., *Chemical Physics Letters* **1985,** 118, 25-8.
77. Stouwdam, J. W.; van Veggel, F. C. J. M., *Nano Letters* **2002,** 2, 733-737.
78. Zang, F. X.; Li, W. L.; Hong, Z. R.; Wei, H. Z.; Li, M. T.; Sun, X. Y.; Lee, C. S., *Applied Physics Letters* **2004,** 84, 5115-5117.

79. Sharma, P. K.; van Doorn, A. R.; Staring, A. G. J., *Journal of Luminescence* **1994,** 62, 219-25.
80. Meshkova, S. B.; Topilova, Z. M.; Bol'shoi, D. V.; Nazarenko, N. A., *Journal of Applied Spectroscopy (Translation of Zhurnal Prikladnoi Spektroskopii)* **2000,** 67, 893-897.
81. Reinhard, C.; Gudel Hans, U., *Inorganic chemistry* **2002,** 41, 1048-55.
82. Zang, F. X.; Hong, Z. R.; Li, W. L.; Li, M. T.; Sun, X. Y., *Applied Physics Letters* **2004,** 84, 2679-2681.
83. Horrocks, W. D., Jr.; Sudnick, D. R., *Journal of the American Chemical Society* **1979,** 101, 334-40.
84. Horrocks, W. D., Jr.; Sudnick, D. R., *Accounts of Chemical Research* **1981,** 14, 384-92.
85. Beeby, A.; Burton-Pye, B. P.; Faulkner, S.; Motson, G. R.; Jeffery, J. C.; McCleverty, J. A.; Ward, M. D., *Journal of the Chemical Society, Dalton Transactions* **2002**, 1923-1928.
86. Tobita, S.; Arakawa, M.; Tanaka, I., *Journal of Physical Chemistry* **1984,** 88, 2697-702.
87. Tobita, S.; Arakawa, M.; Tanaka, I., *Journal of Physical Chemistry* **1985,** 89, 5649-54.
88. Guldi, D. M.; Mody, T. D.; Gerasimchuk, N. N.; Magda, D.; Sessler, J. L., *Journal of the American Chemical Society* **2000,** 122, 8289-8298.
89. Pope, S. J. A.; Coe, B. J.; Faulkner, S., *Chemical Communications (Cambridge, United Kingdom)* **2004**, 1550-1551.
90. Wolbers, M. P. O.; Van Veggel, F. C. J. M.; Snellink-Ruel, B. H. M.; Hofstraat, J. W.; Guerts, F. A. J.; Reinhoudt, D. N., *Journal of the Chemical Society, Perkin Transactions 2: Physical Organic Chemistry* **1998**, 2141-2150.
91. Wolbers, M. P. O.; Van Veggel, F. C. J. M.; Peters, F. G. A.; Van Beelen, E. S. E.; Hofstraat, J. W.; Geurts, F. A. J.; Reinhoudt, D. N., *Chemistry--A European Journal* **1998,** 4, 772-780.
92. *CAChe 6.1.1 ed.; Fujitsu limited; USA* **2003**.
93. Kondo, E.; Hayashi, Y.; Konishi, T.; Hattori, T.; Shoji, J. Tropolone and derivatives as anti-mycoplasma agents, and their preparation. 4950686, 1990.
94. Takase, K., *Bulletin of the Chemical Society of Japan* **1964,** 37, 1460-5.
95. Werts, M. H. V.; Hofstraat, J. W.; Geurts, F. A. J.; Verhoeven, J. W., *Chemical Physics Letters* **1997,** 276, 196-201.
96. Van Deun, R.; Fias, P.; Driesen, K.; Binnemans, K.; Goerller-Walrand, C., *Physical Chemistry Chemical Physics* **2003,** 5, 2754-2757.
97. Iwamuro, M.; Adachi, T.; Wada, Y.; Kitamura, T.; Nakashima, N.; Yanagida, S., *Bulletin of the Chemical Society of Japan* **2000,** 73, 1359-1363.
98. Elliott, J. M.; Chipperfield, J. R.; Clark, S.; Sinn, E., *Inorganic Chemistry* **2001,** 40, 6390-6396.